Progress in Retinal and Eye Research xxx (xxxx) xxx

Contents lists available at ScienceDirect

Progress in Retinal and Eye Research

journal homepage: www.elsevier.com/locate/preteyeres

The role of dark adaptation in understanding early AMD

Ian J. Murray [a,*], Elena Rodrigo-Diaz [a], Jeremiah M.F. Kelly [a], Tariq M. Aslam [a], Humza J. Tahir [a], David Carden [a], Laura Patryas [a], Neil R.A. Parry [b,a]

[a] Vision Science Lab., Faculty of Biology, Medicine and Health, University of Manchester, UK
[b] Vision Science Centre, Manchester Royal Eye Hospital, Central Manchester University Hospitals NHS Foundation Trust, Manchester Academic Health Science Centre, Manchester, UK

ARTICLE INFO

Keywords:
Rhodopsin regeneration
Sensitivity control
Dark adaptation
Drusen
Early/intermediate AMD
Structure versus function

ABSTRACT

The main aim of the paper is to discuss current knowledge on how Age Related Macular Degeneration (AMD) affects Dark Adaptation (DA). The paper is divided into three parts. Firstly, we outline some of the molecular mechanisms that control DA. Secondly, we review the psychophysical issues and the corresponding analytical techniques. Finally, we characterise the link between slowed DA and the morphological abnormalities in early AMD.

Historically, DA has been regarded as too cumbersome for widespread clinical application. Yet the technique is extremely useful; it is widely accepted that the psychophysically obtained slope of the second rod-mediated phase of the dark adaptation function is an accurate assay of photoreceptor pigment regeneration kinetics. Technological developments have prompted new ways of generating the DA curve, but analytical problems remain. A simple potential solution to these, based on the application of a novel fast mathematical algorithm, is presented. This allows the calculation of the parameters of the DA curve in real time.

Improving current management of AMD will depend on identifying a satisfactory endpoint for evaluating future therapeutic strategies. This must be implemented before the onset of severe disease. Morphological changes progress too slowly to act as a satisfactory endpoint for new therapies whereas functional changes, such as those seen in DA, may have more potential in this regard. It is important to recognise, however, that the functional changes are not confined to rods and that building a mathematical model of the DA curve enables the separation of rod and cone dysfunction and allows more versatility in terms of the range of disease severity that can be monitored. Examples are presented that show how analysing the DA curve into its constituent components can improve our understanding of the morphological changes in early AMD.

1. Introduction

The link between early Age Related Macular Degeneration (AMD) and poor night vision is well established. The abnormality is particularly evident when the eye is recovering sensitivity in darkness after being exposed to a bright light. The time course of recovery, known as the dark adaptation (DA) curve, is widely regarded as an accurate assay of the integrity of the health of the outer retina. As such, the technique could provide insights into the pathophysiology of non-neovascular AMD and act as a biomarker of the condition. A more complete understanding of the link between rod and cone photoreceptor sensitivity recovery and the development of the disease will enable the efficacy of future AMD management strategies to be assessed.

The aim of the paper is to describe the fundamentals of DA in the context of the way it is compromised in early AMD. Space does not permit a comprehensive review of the underlying physiology. Rather we are concerned with capturing the extent to which this technique is relevant to advancing our understanding of the disease. The primary goals of this paper are as follows. Firstly, we briefly review what is known of the molecular and biochemical processes that control sensitivity recovery following exposure of the eye to a bright light and the resultant photoisomerisation of the visual pigments. The molecular reactions generated in the outer retina as sensitivity is restored from the ensuing profound transient loss of vision are of particular relevance. They represent a unique challenge to the efficient co-operation between the different structures of the outer retina and appear to be particularly susceptible in the early stages of AMD.

Second, we discuss methodology. Monitoring sensitivity recovery

* Corresponding author.
E-mail address: ian.j.murray@manchester.ac.uk (I.J. Murray).

https://doi.org/10.1016/j.preteyeres.2021.101015
Received 21 April 2021; Received in revised form 24 September 2021; Accepted 29 September 2021
Available online 6 October 2021

involves measuring thresholds over time and plotting and analysing the resulting multicomponent recovery function. Some of the technical limitations and psychophysical issues associated with obtaining a DA curve are highlighted. Maintaining accurate control of stimulus intensity over a wide dynamic range and minimising the length of time of the test are of major concern. The DA curve is non-linear so accurate determination of the parameters requires complex analysis. A novel analytical approach to this problem is presented that allows extremely rapid modelling of DA data.

Finally, we review the psychophysical observations reported using Dark Adaptometry in the normal ageing eye and relate these to those described in AMD. Impaired recovery of sensitivity after a bleach has been consistently shown to be the primary functional impairment in the early stages of AMD. Other aspects of visual function have also been shown to be compromised and it is now appropriate to bring together the functional and morphological deficits to identify the conditions under which they do and do not match.

The main problem addressed in the paper is how to test the proposition that a particular pathophysiological change induces a specific functional defect. In severe AMD, loss of visual function and the disorganisation of the outer retinal structures are largely irreversible. It is therefore crucially important to appreciate that, in the early stages of the disease, although functional loss is hardly discernible, there is a real prospect of impeding disease progression. Indeed, many patients have signs of early AMD that remain unchanged for many years. At present, grading early AMD relies on categorisation of morphological changes whilst visual loss is largely ignored. It is important, therefore, to explore the detailed functional abnormalities and their link with structural changes as revealed by techniques such as retinal imaging. Abnormal DA is the earliest detectable visual change in AMD so a sound understanding of all aspects of DA can be expected to generate robust and verifiable observations regarding the intricacies of the structure-function relationship in the early stages of the disease.

2. Overview of photoreceptors

2.1. Rods and cones

In this section we briefly highlight the features of photoreceptors that are relevant to later sections of the paper. Vision begins with the absorption of light by photopigments located in the outer segments of two distinctly different photoreceptor types, the rods and the cones. Despite their different biology, the functional overlap between the two is seamless so that they are capable of signalling a remarkable 10 orders of magnitude (Barlow, 1972). Interestingly, this is a close match to the 11 orders of magnitude spanned by the daylight cycle (Wyszecki and Stiles, 1982). In humans, vision is thought of as being dominated by cone-mediated photopic vision, yet cones constitute less than 5% of the retinal photoreceptor count and are predominant across only a small central region of the retina (Curcio et al., 1990; Osterberg, 1935).

2.2. Spatial distribution

The distribution of photoreceptors is highly heterogeneous, with the central foveolar (1.25° diameter) rod-free zone being tightly packed with cones which decrease rapidly in density with increasing eccentricity (Osterberg, 1935). As the number of cones decrease, rod density increases so that there are equal numbers of rods and cones in a horizontal oval of diameter around 1.75°. Beyond this eccentricity, cone density is reduced and rods increase to a peak density at around 20°, after which there is a steady decline. As reported in Curcio et al. (1990), there is marked individual variation in the central cone mosaic, ranging from 100,000–324,000 cones/mm^2. However, the total photoreceptor count is probably consistent across populations. The widely accepted typical numbers are ~6 million cones and ~120 million rods. Importantly for the present work, rods outnumber cones by 9:1 in the central (20°) macular region.

2.3. Regulation of sensitivity

Photoreceptors are rarely called upon to detect a target against a totally black background. Both rods and cones exhibit the ability to decrease sensitivity in the presence of a background. This essentially shifts the entire operating range to higher intensities so that sensitivity, the ratio of a just-detectable stimulus increment to its background, is approximately inversely proportional to background intensity. This principle, fundamental to all sensory systems, was first described by Weber in the 1800's (Weber, 1834). It is crucial for everyday perception in that constant adjustment to the background lighting means objects can be detected at almost the same contrast despite large changes in ambient illumination.

The Weberian principle was established for photoreceptors in some now classical experiments with primate eyes (Boynton and Whitten, 1970). When backgrounds are switched off, cones recover rapidly, but rods recover more slowly to the dark potential level. For rods, the linearity of signal detection and their very high sensitivity mean that response amplitude reaches maximum values at relatively low luminance levels of around 100–200 cd m^{-2}. At greater levels of intensity, it is commonly thought that rods saturate and do not respond to any visual stimuli but in some situations rods might still operate in the presence of much higher backgrounds (Tikidji-Hamburyan et al., 2017).

2.4. Cones

Cones return extremely rapidly to normal sensitivity after exposure to different light intensities. They detect contrast increments as small as 0.5% in both spatial and temporal domains. Due to their close packing in the rod-free foveola, cones facilitate high spatial acuity of the order of 35–40 c/deg. This matches the foveal intercone distance of 0.5 μm (Snyder and Miller, 1977). They respond rapidly to variations in light intensity (van Hateren and Lamb, 2006) and are thereby capable of detecting flicker up to 100 Hz in optimum conditions. There are three cone types, identified by the different absorption spectra of their opsins. These enable the discrimination of perhaps 2 million colours, by virtue of a differencing mechanism called cone opponency (Hurvich and Jameson, 1955; Ingling, 1977). See Shevell and Martin (2017) for an excellent multidisciplinary commentary. Despite markedly reduced numbers in the peripheral field, cone-based colour vision, albeit in a reduced form, persists to an eccentricity of at least 18° (Parry et al., 2006).

2.5. Rods

The single most important characteristic of rods is that they are capable of responding to extremely low light levels (Hecht, 1937). The scotopic system takes advantage of the very large numbers of rods by forming a powerful spatial pooling mechanism and this, together with their other properties discussed below, enables rods to respond to individual photons (Baylor et al., 1979). Other aspects of vision are inevitably sacrificed in this arrangement; rods are relatively sluggish, taking tens of minutes to reach maximum sensitivity during recovery from bright lighting conditions. They have poor visual acuity and an order of magnitude worse contrast sensitivity than cones. Cones, however, are much noisier at an individual level than rods (Robson and Frishman, 1998).

3. OPSIN regeneration and phototransduction: anatomical and molecular considerations

Here we briefly describe the molecular steps underlying sensitivity recovery. The dynamics of photopigment regeneration are discussed in the context of the time course of the DA curve. The components of the

DA curve are explained in terms of the molecular biology and in particular it is established that the slope of the second rod-mediated component is an accurate measure of the concentration of 11-*cis*-retinal in the retinal pigment epithelium (RPE).

3.1. Photoreceptors and their intimate relationship with the RPE

The main steps in opsin regeneration have been known for some time and there are many excellent reviews that provide more detail, for example (Fain et al. (2001), Lamb and Pugh (2004); Reuter (2011); Saari (2012)). We will begin by describing the structures of the outer retina and their relationship with the RPE and the vascular supply. This discussion is concerned mainly with the human retina but much of the basic biology is based on work with other mammalian species.

Photoreceptors are divided into five main regions: outer segment (OS), connecting cilium (CC), inner segment (IS), nuclear region and synaptic region. In rods, the OS contains around 800 double lamellar disc membranes packed with rhodopsin molecules. Cone outer segments are quite different. They are composed of tight involutions of the plasma membrane to form sacs filled with cone opsins. This arrangement means they are in direct contact with the inter-photoreceptor matrix (IPM) and can rapidly exchange nutrients and metabolites with that structure, as described in Mustafi et al. (2009). Photoreceptor outer segments form invaginations into the long apical microvilli of the RPE, illustrated in Fig. 1.

The RPE is a monolayer of pigmented cells forming the outermost layer of the retina. Its basal membrane faces Bruch's membrane which separates it from the capillary layer of the choroid, the choriocapillaris. This intimate relationship with the photoreceptors and the anatomic proximity of Bruch's membrane makes the RPE critical to the issues explored in this paper. The integrity of the photoreceptors is entirely dependent on the normal functioning of the RPE. As described in Lamb and Pugh (2004) and Strauss (2005), the RPE protects the retina from the choroidal circulation, acting as the blood-brain barrier. It transports essential materials such as Vitamin A metabolites, it performs phagocytosis of the disposed tips of outer segments and synthesises the vital chromophore 11-*cis*-retinal, as described below. It also maintains the extra-cellular space, which contains the inter-photoreceptor matrix (IPM). In the peripheral retina, individual cones and around 20 to 30 rods share microvilli from the apical surface of a single RPE cell.

The functional interdependence of photoreceptor outer segments and the RPE follows from their embryonic development (Strauss, 2005). It explains the apparently paradoxical configuration of the mammalian retina, in which the photoreceptor layer is positioned furthest from light entering the pupil.

3.2. Bruch's membrane and the choriocapillaris

Bruch's membrane is a five-layered extracellular matrix strategically located between the RPE and the choriocapillaris, as illustrated in Fig. 1. Essentially, it is a molecular sieve, composed of an RPE basement layer, inner and outer collagenous layers and an elastic layer bound distally by the choriocapillaris basement membrane. In younger eyes, it is around 2 μm in thickness but this increases with age, as discussed in section 5. Its

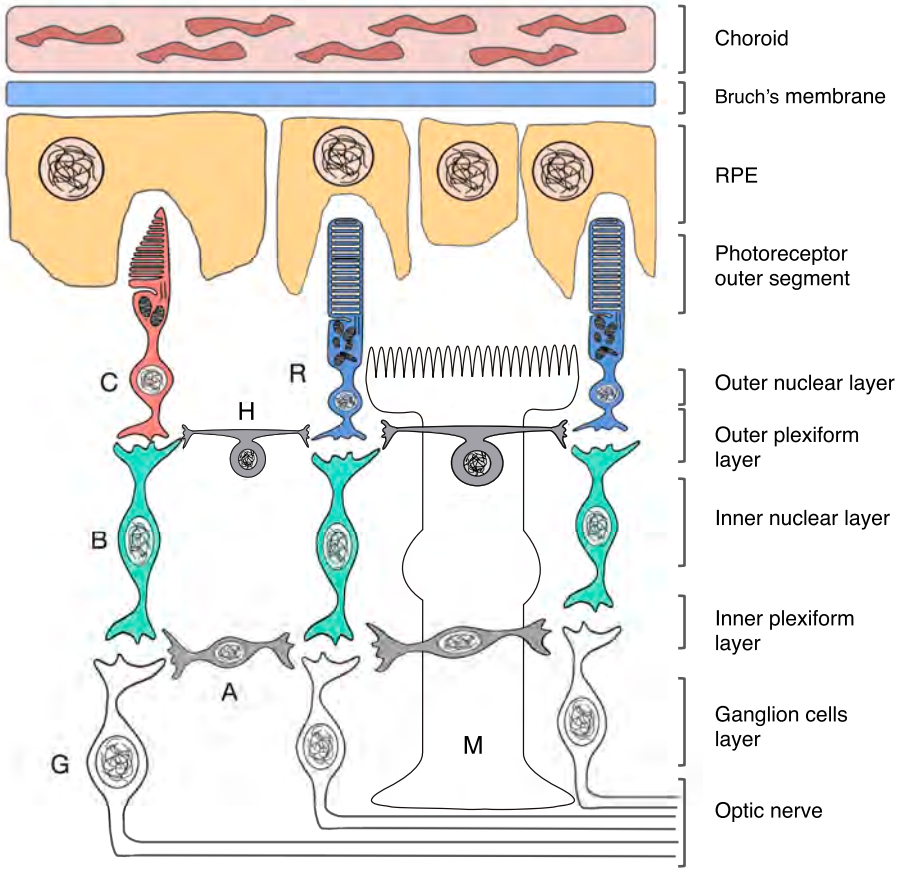

Fig. 1. The intimate relationship between photoreceptors and the microvillae of the RPE. Note the proximity of Muller cells to rods and to cones. C- Cone, B – Bipolar cell, H – Horizontal cell, R – Rod, A – Amacrine cell, M Muller cell. (Rodrigo-Diaz, 2017).

primary role is to regulate the reciprocal exchange of nutrients, oxygen, biomolecules and waste products between the retina and the systemic circulation (Booij et al., 2010).

There are substantial differences between the macula and the periphery, as reported by Chong et al. (2005), the elastin layer being much thinner and more porous in the macula than the periphery. Diffusion across Bruch's membrane is primarily passive, depending on the composition of the molecules passing across the membrane and the hydrostatic pressure on both sides. Biomolecules transported from the choroid to the RPE are nutrients, lipids, pigment precursors (mainly vitamin A) and oxygen. Those passing in the other direction from RPE to choroid are CO_2, water, ions, oxidised lipids and cholesterol, visual cycle waste products and partly digested fragments of photoreceptor outer segments (Bok, 1993). There is no doubt that Bruch's membrane undergoes marked changes in normal aging. These are well documented and their implications for impaired function of the RPE are discussed in Booij et al. (2010).

3.3. Visual pigments

Visual pigments belong to the family of retinylidene proteins, whose property is that they facilitate the conversion of electromagnetic radiation into a biochemical cascade within cells. Visual pigment molecules are located in the cell wall of the photoreceptor outer segments. They are composed of a spectrally-tuned opsin protein covalently bound to a chromophore (11-*cis*-retinal) via a Schiff base. 11-*cis*-retinal is a photosensitive derivative of Vitamin A. It acts as the light-absorbing component of all known visual pigments. Opsins in themselves are not light sensitive. Light absorption induces isomerisation of a double bond in the chromophore that triggers a conformational change and subsequent activation of cellular signalling pathways. (see Fig. 2).11-*cis*-retinal binds the opsin as an inverse agonist, locking it in its inactive form. The rod photopigment molecule is rhodopsin. The story in cones is similar but they have their own opsin component combined with 11-*cis*-retinal. In rods, isomerisation of 11-*cis*-retinal to all-*trans*-retinal results in the formation of the active form of rhodopsin called metarhodopsin (or R*) which triggers the transduction cascade.

3.4. The classical visual cycle

The first step in seeing is the absorption of a photon by a visual pigment molecule. When a photon is absorbed, 11-*cis*-retinal is instantaneously isomerized to all-*trans*-retinal and the new conformation activates the opsin (Palczewski and Kiser, 2020); Lamb and Pugh (2006).

The photo-activated form of the molecule, metarhodopsin or R*, triggers the G-protein transduction cascade, described below, causing the ion channels of the cell's plasma membrane to close and a reduction in the circulating current. As is well known, the subsequent hyperpolarisation of the photoreceptor is proportional to the intensity of the light signal. See Lamb and Pugh (2006) for an excellent account of this process.

As stated above, the opsin molecule must be recharged with 11-*cis*-retinal in order to regain photoactivity. The details of this process are well documented (Fain et al. (2001); Lamb and Pugh (2004); Saari (2012)). In order to avoid overlap with others, we present only a brief synopsis here. Historically, much of the understanding of the visual cycle is based around the rod photopigment rhodopsin. Note that recent evidence points to the adjunctive role of the non-visual opsin Retinal G protein-coupled receptor (RGR) in regulating the regeneration of 11-*cis*-retinal. RGR is found in RPE and Muller cells and plays a role in photopic and scotopic sensitivity recovery (Choi et al., 2021). Whilst cones regenerate some of their photopigments through the classical pathway, they also access an alternate system, based on the inner retina and Muller cells, which we discuss in section 3.5. For simplicity we divide the classical visual cycle into three stages.

3.4.1. Stage 1. removal of 11-cis-retinal

The different reactions and their relationship to the anatomical configuration between rods and RPE cells are shown in Fig. 3. Following absorption of a photon, the all-*trans*-retinal is released from the activated opsin and is transported to the cytoplasmic disc surface (Liu et al., 2000). In the cytoplasm it is reduced to all-*trans*-retinol (Vitamin A). At this stage it is bound to the interphotoreceptor retinoid binding protein (IBRP) which chaperones it across the sub-retinal space and allows it to enter an RPE cell (Bunt-Milam and Saari, 1983; Wu et al., 2007).

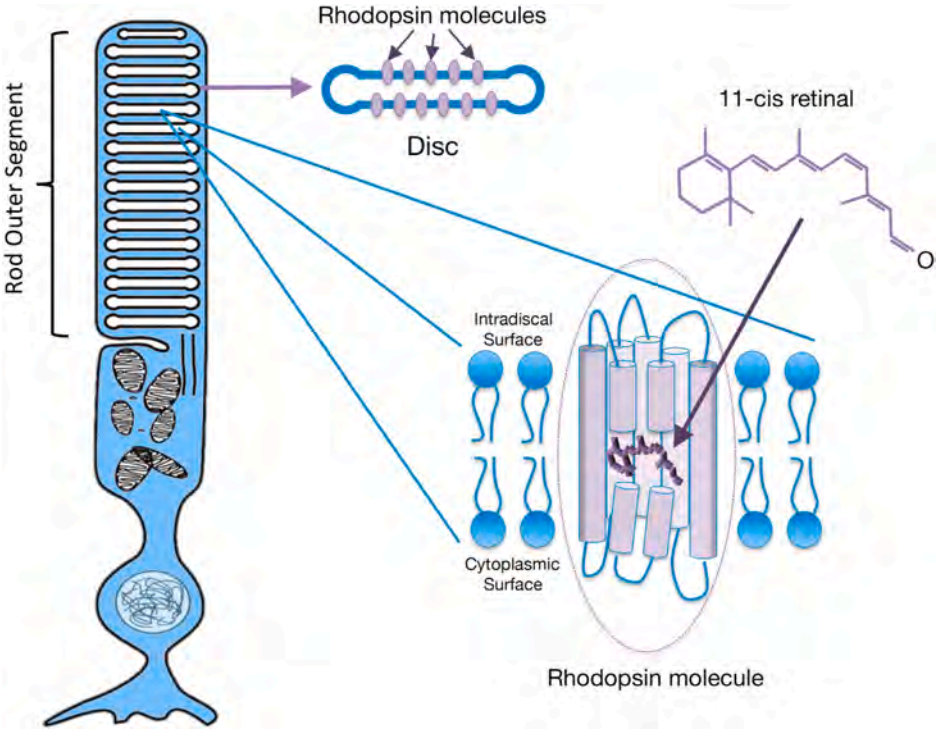

Fig. 2. Rhodopsin located in rod outer segments, illustrating the locked form of 11-cis- retinal (Rodrigo-Diaz, 2017). Redrawn from Hargrave (2001)
Note that all-*trans*-retinal is required to activate opsin but the opsin must subsequently be released so that it can bind new 11-*cis*-retinal and thus form a regenerated visual pigment molecule. In rods, the process of regenerating visual pigment molecules requires an ensemble of enzymatic steps called the visual cycle and this is described below.

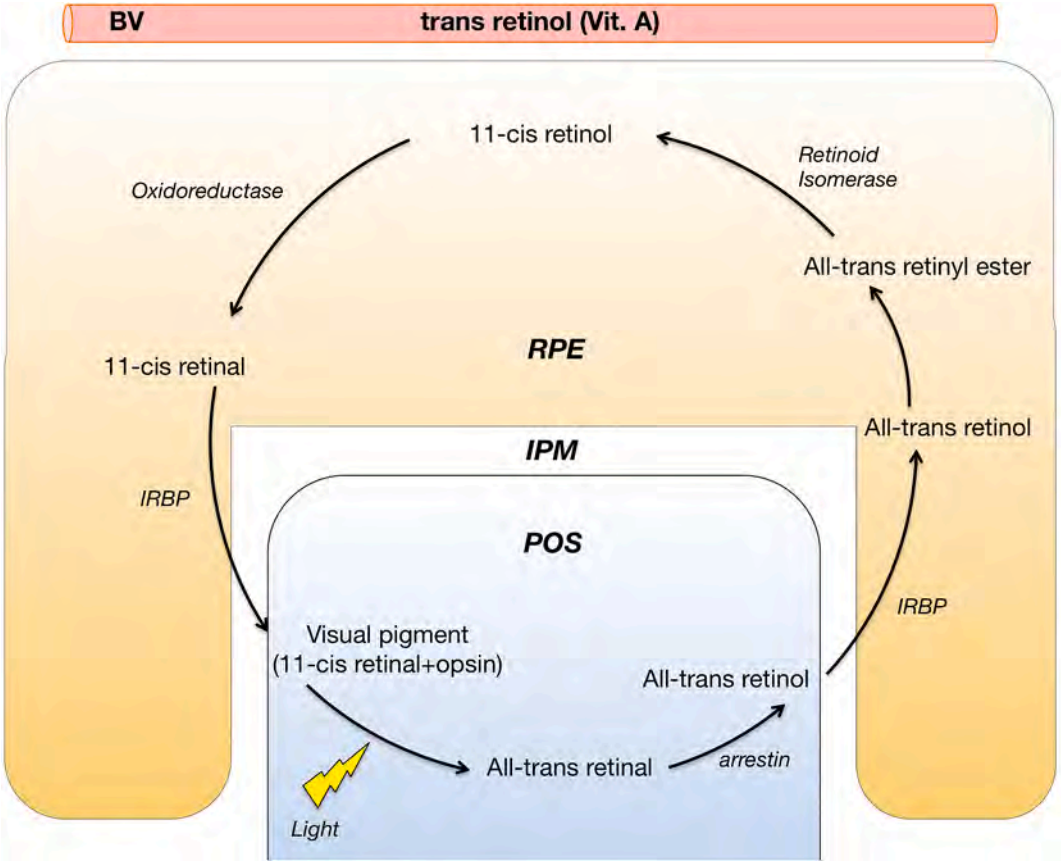

Fig. 3. The classical visual cycle. RPE Retinal pigment Epithelium. IPM interphotoreceptor matrix. POS Photoreceptor outer segment. IRBP Interphotoreceptor retinoid binding protein. Note that IRBP plays a chaperone role in both the removal stage and the delivery and synthesis stage of all-*trans* retinoid (Rodrigo--Diaz, 2017).

3.4.2. Stage 2. role of the RPE

In the RPE, three enzymatic reactions convert all-*trans*-retinol to 11-*cis*-retinal: first, all-*trans*-retinol is esterified to form all-*trans*-retinyl esters (Saari et al., 1982). Second, all-*trans* esters are hydrolysed to yield 11-*cis*-retinol, via the RPE65 protein (Saari et al., 2001). Finally, 11-*cis*-retinol is oxidised to 11-*cis*-retinal by retinol dehydrogenase (Simon et al., 1995). During this phase, all-*trans*-retinol from the systemic circulation can enter the visual cycle through the basal surface of RPE cells. This explains the well-known importance of dietary vitamin A to vision.

3.4.3. Stage 3. return of 11-cis-retinal to photoreceptor outer segment

The newly generated 11-cis-retinal is then shepherded back into the rod outer segment across the subretinal space, again by IRPB, which protects it from isomerisation. There is some ambiguity in the exact order of the steps leading to the recovery of activated rhodopsin (Weiss, 2020). In the outer segment, the 11-*cis*-retinal is covalently bound to a lysine residue in the chromophore-binding pocket of opsin to produce a regenerated visual pigment molecule to complete the visual cycle. See Lamb and Pugh (2004). Note that IRBP is one of the most abundant proteins in the eye as might be expected given that it acts as a chaperone for both the removal of all-*trans*-retinol from, and the delivery of 11-*cis*-retinal to, the outer segments.

3.5. The cone visual cycle

The rate of visual pigment bleaching in sunlight is much too high to be sustained by the rate at which all-*trans*-retinal is converted to 11-*cis*-retinal by the classical retinoid cycle. Yet cones readily support vision under these circumstances. This enduring puzzle was addressed in a seminal paper by Mata et al. (2002). Earlier, there had been frequent reports that cone pigment regeneration does not rely on the classical visual cycle. For example, it had been reported that cone pigments, but not rod pigments, can regenerate in frog retina isolated from the pigment epithelium (Goldstein and Wolf, 1973). Also, there was evidence that the Muller cell, the major glial cell located adjacent to photoreceptors (see Fig. 1), can isomerize all-*trans*-retinol to 11-*cis*-retinol (Das et al., 1992). Following experiments with cone-dominated animals such as chicken and ground squirrels, Mata et al. (2002) proposed the pathway illustrated in Fig. 4.

All-*trans*-retinol is absorbed by Muller cells where it is converted directly to 11-*cis*- retinol. It is then released from the Muller cells and taken up in the inner segments of cones where it is oxidised to 11-*cis*-retinal by a cone-specific dehydrogenase. This unique ability of Muller cells to regenerate 11-*cis*-retinal was first described by Jones et al. (1989). It is interesting to note the close proximity of Muller cells to the apical microvilli of RPE cells. (Fig. 1). The latter contain a retinoid binding protein with a high affinity for 11-*cis* retinoids called CRALBP (Bunt-Milam and Saari, 1983).

The retinal version of the visual cycle enables cones to remain responsive over a wide luminance range because at least some of the pigment is constantly being regenerated. This more direct pathway would have many benefits over the RPE-based pathway; first, it is around 20 times faster than the RPE-based pathway (Arshavsky, 2002) and second, rods cannot oxidise 11-*cis*-retinol to 11-*cis*-retinal, thus preventing them from absorbing the oxidised retinoids under daylight conditions and effectively poaching the regenerated retinoid. See Lamb (2016) for an interesting evolutionary perspective on this point. This would be important in rod dominated retinae such as humans. The classical pathway is compared with the cone-only pathways in Fig. 4. It

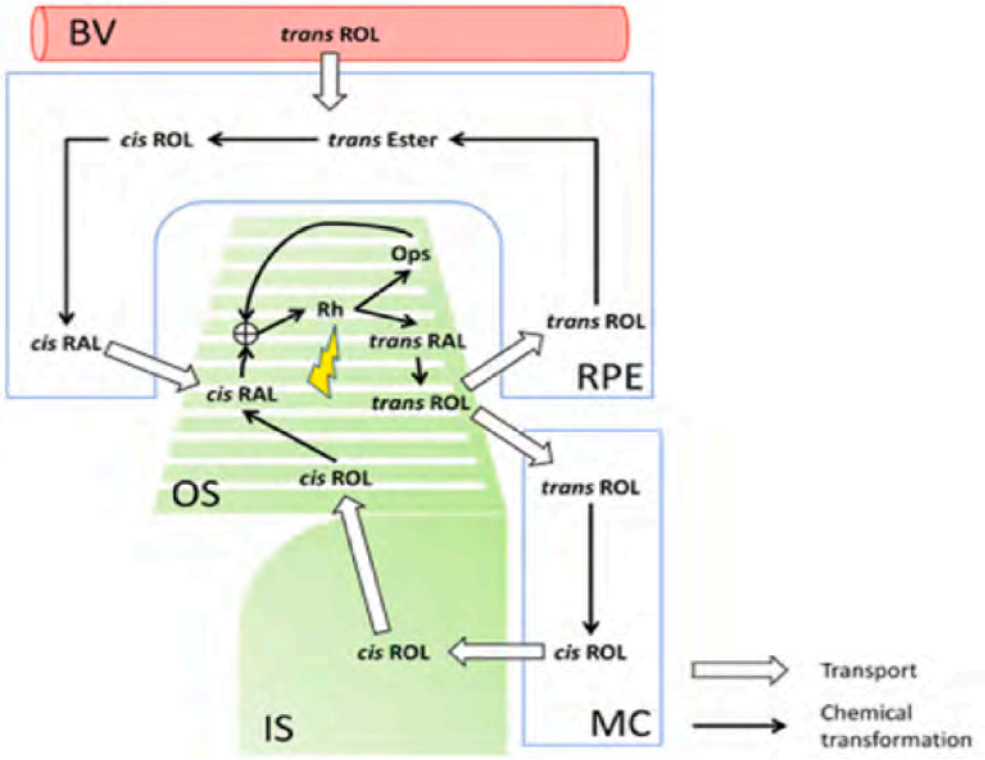

Fig. 4. Comparison of direct and RPE-based pathways for the regeneration of cone opsins. MC - Muller Cell. RPE Retinal Pigment Epithelium. OS- outer segment. IS- inner segment. ROL retinol. RAL-retinal (Wang and Kefalov, 2011).

should also be mentioned that cone free opsins do not shut off circulating current as does rod free opsin. This means that cones, unlike rods, can continue to respond to light when they contain large amounts of free opsin.

3.6. Overview of transduction

Following the absorption of a photon, the visual pigment molecule is isomerized to its all-*trans* configuration and this activates phototransduction. There follows a very rapid cascade of intermediaries and rhodopsin is transformed to its active state known as R*. Within milliseconds, R* leads to a depletion in the concentration of the cytoplasmic messenger cyclic guanosine monophosphate (cGMP) via the G protein transducin and phosphodiesterase (Lamb and Pugh, 2004). All--*trans*-retinal then dissociates from the opsin leaving the chromophore pocket empty. The opsin is now 'bleached', in that it becomes colourless. In the dark, cGMP is in equilibrium between synthesis and hydrolysis. In response to light, the rate of hydrolysis of cGMP increases, leading to a reduction in its concentration.

Reducing the concentration of cGMP means that it unbinds from the ion channels in the cell's plasma membrane, causing these channels to close, and thus causing a reduction in circulating current and consequent hyperpolarisation. This graded visual signal is transmitted via the synaptic cleft to the downstream neural pathway. It is essential that the phototransduction cascade is deactivated and this occurs as a result of the phosphorylated site in R* being tightly bound by the protein arrestin. Although this prevents further activation by transducin, note that the photopigment returns only slowly to its activated state. It cannot signal the arrival of another photon until its all-*trans* retinoid has been replaced by a new molecule of 11-*cis*-retinal.

After activation of a significant proportion of rhodopsin molecules (for example by a bleaching flash or background) it is at this stage of removal of so-called free opsin where the rate-limited bottleneck in sensitivity recovery occurs. The phenomenon is discussed below but suffice to say here that the rate of removal of opsin saturates for bleach intensities greater than around 20%. This is due in part to residual arrestin remaining bound to the opsin.

3.7. From molecules to vision: the dark adaptation curve

As is well known, exposure to a high intensity light results in a profound loss in sensitivity of around 5 log units (Hecht, 1937). In total darkness, recovery is biphasic. The data are typically plotted in semi log co-ordinates with the y-axis expressed as Log_{10} threshold luminance and the x-axis in minutes after the offset of the bleach (see Fig. 5). For intense bleaches (see 3.7.1) there is an initial cone-mediated exponential phase leading to a conspicuous inflexion point, α, sometimes called the rod-cone break. It represents the transition from cone-to rod-mediated sensitivity, usually at around 3 log units above absolute threshold and at around 8–10 min.

The point on the sensitivity axis at which α occurs defines the cone threshold, essentially the maximum sensitivity of the cone photoreceptors for the particular viewing conditions. Stimulus variables that influence cone sensitivity include target eccentricity, size and wavelength and the intensity and wavelength of the background. The time to reach α is closely related to the bleach intensity.

3.7.1. Intensity of the bleach

The intensity of the bleach is specified by the extent to which the full complement of visual pigment is 'bleached' or deactivated. The fraction of bleached rhodopsin is proportional to the incident energy *I,* and its duration t ($t < 40$ s). The relationship between intensity, *I,* in scotopic trolands and pigment remaining, *po,* is based on a series of retinal densitometry measurements in human eyes as described in Rushton and Powell (1972), The equation below is derived from curve fits to these data:

$$log_{10}\left(log_{10}\left[\frac{1}{p_0}\right]\right) = log_{10}(It_0) - 7.3 \quad (1)$$

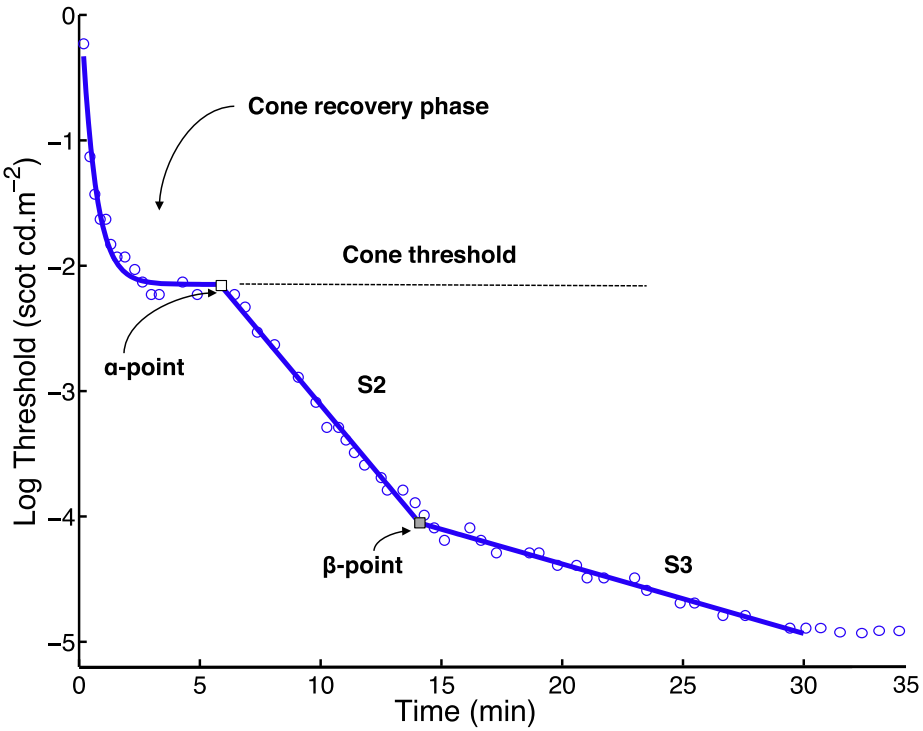

Fig. 5. Typical DA curve for a young, healthy observer measured inferiorly at 5.5° eccentricity, following a bleach of 97%. The α point, S2 phase, β point and S3 phase are indicated. Note the final phase of S3 is not included in the modelling (Rodrigo-Diaz, 2017).

where *po* is remaining pigment.

*It*0 = incident light energy expressed in scot. Td.s.

For example, for a 98% bleach, intensity of 7.6 log scot Td. s for 0.001 s is required.

3.8. Components of the DA curve

There follows a brief description of the components of the DA curve, plotted in the conventional way with Log threshold vertically and time horizontally, as in Fig. 5. Note that the cone coefficient represents sensitivity immediately after the offset of the bleach but this has no real physiological value. It is used as a free variable during the fitting process. The different components are fully discussed elsewhere (Lamb and Pugh, 2004).

3.8.1. The cone threshold

Cones recover extremely quickly following a bleach. The cone plateau occurs at about 3 log units above absolute threshold. The shape of the recovery function can be fitted with an exponential with a time constant, θ_3, of around 2 min (equation (2)). The cone threshold can be elevated by stimulating the cones, for example with a dim red background, which essentially impedes their recovery to maximum sensitivity. This red background would be close to invisible to the rods but would raise the cone plateau thereby shortening the transition time to rod mediated recovery, α. This idea is discussed in section 4.4.

$$Thresh = \theta_1 + \theta_2.\exp\left(-\frac{t}{\theta_3}\right) \quad (2)$$

where.

Thresh = threshold,
θ_1 = cone threshold,
θ_2 = Cone coefficient
θ_3 = cone time constant.
t = time

3.8.2. The second rod-mediated stage, S2

S2 is the second of the rod-mediated sections of the curve. Under normal conditions, the first section, S1, is not visible because of the presence of the cone section. Sensitivity improves linearly and, as discussed below, the rate of this recovery is independent of bleach for a range of bleach intensities from 2% to 98%. Lamb (1981) reports the range of time constants corresponding to these bleaches as largely unchanged between 105 s and 108 s. The increase in threshold is linear in a semi $\log_{10}$ graph, indicating that it is an exponential function.

For example, the exponential decay of 0.24 log units per minute corresponds to a time constant of $\log_{10}(e)/0.24 = 108$ s. S2 is regarded as a universal characteristic of human sensitivity recovery in a young healthy individual (Lamb and Pugh, 2004).

3.8.3. Alpha (α)

There is a prominent inflexion in the DA curve as the transition from cone detection to rod detection occurs. The time to reach this point is strongly dependent on bleach intensity. As discussed in detail below, the rods take longer to reach the sensitivity of the cone plateau as more of the rhodopsin is bleached. In normal observers α (the rod-cone break) occurs at around 8 min after a bleach of around 90%.

3.8.4. The third rod-mediated stage, S3

After 15 min or so, corresponding to about 90% sensitivity recovery, there is a further change in time constant which suggests that the dynamics of recovery are no longer controlled by S2. The slope changes to around 0.06 log units per minute, corresponding to a time constant of 6–7 min. To a first approximation, S3 can be regarded as linear. However, Pugh (1975) clearly shows that the data asymptote with the x-axis. It is likely that this stage of recovery is heavily influenced by the exponential decline in opsin concentration. The exact value of S3 is difficult to estimate because, as discussed in Lamb and Pugh (2004), it is linear for around 15 min after β, the rod-rod transition point and then levels off as it approaches the absolute threshold. For the three highest bleaches in Pugh (1975), the time constants of S3 were 6.8, 7.0 and 6.8 min. As absolute threshold is approached, the dark light will sum with

component S3 and this will tend to 'round out' the function to give the familiar asymptotic shape. This is depicted in Fig. 5 by the final data points. These are not generally included in the modelling of the curve described in Section 4.

3.9. Some fundamentals of sensitivity recovery

Below we consider some issues that attracted much attention and controversy in the early days of investigating the DA curve. From the experimental evidence gathered in the 1930's, it was clear that the characteristics of the curve were in some way reflecting the regeneration of the photopigments and that the rods were recovering slowly due to the molecular processes controlling rhodopsin regeneration. There are three important issues to be considered, relating to the speed of recovery, the mechanism of loss of sensitivity and the role of the background.

3.9.1. DA is slow

First, we might ask why the rod mediated phase of the DA curve is so slow. One important consideration is that some biochemical species released during recovery are toxic and if the process were faster these would reach higher concentrations, possibly resulting in retinal damage (Lamb, 2016). All species recover sensitivity in the dark over a period of tens of minutes. In contemporary urban environments, we are rarely required to reach maximum sensitivity, but the benefits of a separate retinal circuitry capable of detecting very low levels of light, which has been available to animals for many millennia, would have substantial survival advantages. The trade-off has always been that the rod system integrates over long periods of time in order to achieve high sensitivity. The actual time course has probably evolved to match the fading of evening light, as discussed in Lamb (2016).

3.9.2. Raised thresholds are due to a photoproduct of bleaching not depleted rhodopsin

A second point is that, as reported many years ago, the reduction in sensitivity in no way represents loss of rhodopsin (Hecht, 1937). This point is illustrated by the fact that a bleach of 20% of the rhodopsin results in a disproportionate loss (around 3 log units or a factor of 1000) in sensitivity. Instead of rhodopsin insufficiency, it is well known that the primary reason for raised threshold is the *presence* of a photoproduct of bleaching and it is now accepted that this product is 'free opsin'. Free opsin is the protein produced when all-*trans*-retinal has detached from the visual pigment molecule and before fresh 11-*cis*-retinal recombines with the opsin to regenerate rhodopsin. Note that the term 'free opsin' may be misleading. Schadel et al. (2003) suggested that opsin may never be totally free of retinoid. We use the term opsin removal to indicate that this is the point when opsin recombines with 11-*cis*-retinal.

3.9.3. Equivalent background intensity

The third point relates to the perception of the observer immediately the bleaching light is turned off and again the observation has a venerable history. Stiles and Crawford (1932) reported that the observers experience the sensation of an equivalent background light that fades gradually after the extinction of the bleaching light. It was thought that bleaching generated a product or products that mimic light. Subsequently it was shown that this effect was internal to the photoreceptors, suggesting that the substance responsible for raising threshold was simulating the activation of R* and thereby triggering the transduction cascade. Lamb (1981) suggested that the threshold-raising substance which causes the so-called 'equivalent background intensity', must decline exponentially, thereby producing the linear reduction in the threshold when plotted on a Log_{10} *vs* time graph. The main point is that the elevation of thresholds is proportional to the concentration and subsequent removal of photoproduct. This in turn is controlled by the process of phototransduction, as discussed in Section 3.6.

3.10. High and low intensity bleaches generate fundamentally different DA curves

A crucial issue to emerge during the early exploration of DA was the marked influence of the intensity of the bleach on the duration and shape of the function (e.g. Pugh, 1975). The data presented in Fig. 6A and B are from Patryas et al. (2013). Fig. 6A plots Log_{10} threshold against time and shows data for 6 different levels of bleach intensity from 16% to 100% of the total. The small (16%) bleach reveals three distinct sections. The first, particularly fast, component is linear and has a slope of 5.5 decades/min, a time constant of 4.8s. This component was said by Lamb (1981) to be mediated by the first rod-specific component and he assigned it to a hypothetical 'substance 1', hence the term S1.

There is a second component with a slope of about 0.24 decades/min corresponding to a much longer time constant of around 105s. Crucially, this second component, referred to by Lamb (1981) as S2, has a very similar slope for all bleaches. As discussed above, he showed that it is independent of the bleach intensities from 2% to 98% (see his Fig. 2). However, it is evident that, although the different bleaches generate values of S2 with the same slope, their impact on recovery is fundamentally different for bleach intensities above and below around 20%.

Examination of Fig. 6A shows that, as bleach intensity increases, it has a disproportionate effect on time of recovery. This can be seen in Fig. 6B wherein the time to recover to a criterion level of −2.5 log units (depicted by the horizontal line in Fig. 6A) is plotted against bleach intensity. It is apparent that the time to recover to this level is very rapid for small bleaches and that, after a watershed level of 20%, it increases proportionally with the bleach. At higher intensity bleaches, S2 behaves quite differently. It looks like the chemical intermediaries from the bleach responsible for raising threshold are removed from the rod outer segment exponentially, with a time constant of 1.8 min, as discussed in Lamb and Pugh (2004). That is, each increase in bleach induces a proportionate elevation of the recovery function resulting in a straight line on the semi-log plot.

For more intense bleaches, the marked increase in initial threshold elevation can be seen if the lines drawn through the data in Fig. 6A are extrapolated to time zero. For the 96% bleach, the initial threshold is some 5000x higher than the equivalent threshold at time zero for the 16% bleach, even though the bleach has increased by only a factor of 25. As first reported in Lamb (1981), this is due to a systematic delay in the removal of photo product and represents classic rate-limited behaviour. This is quite distinct from unimolecular (exponential first-order) reactions. This additional step or delay must be linear and is likely to be linked to delivery of 11-*cis*-retinal from the RPE. Lamb and Pugh (2004) show that an extra 7 s is required for each 1% increase in bleach intensity, as revealed in their Fig. 7. They point out that the same rate-limited kinetic process underlies regeneration of rhodopsin, psychophysical DA and rod photocurrent recovery.

To summarise, weak bleaches reveal two components of threshold elevation and these have decay time constants of around 5 s and 100 s. In the case of more intense bleaches, the recovery time to the rod region is linearly related to fraction bleached. As a result of comparing sensitivity recovery with bleach intensity and assuming the equivalent background is caused by chemical intermediaries, Lamb (1981) proposed a quantitative model linking the hypothetical substances S1, S2 and S3 with the three components of sensitivity recovery.

3.11. Linking the time course of recovery with the underlying molecular reactions

As discussed above, it has been thought for many years that sensitivity recovery is linked to the regeneration of visual pigment and that this in turn is controlled by the removal of free opsin and the concentration of 11-*cis*-retinal (Rushton and Henry, 1968). Subsequently this so called 'equivalent light hypothesis' found further support when Pepperberg et al. (1978) showed that the delivery of 11-*cis*-retinal restored

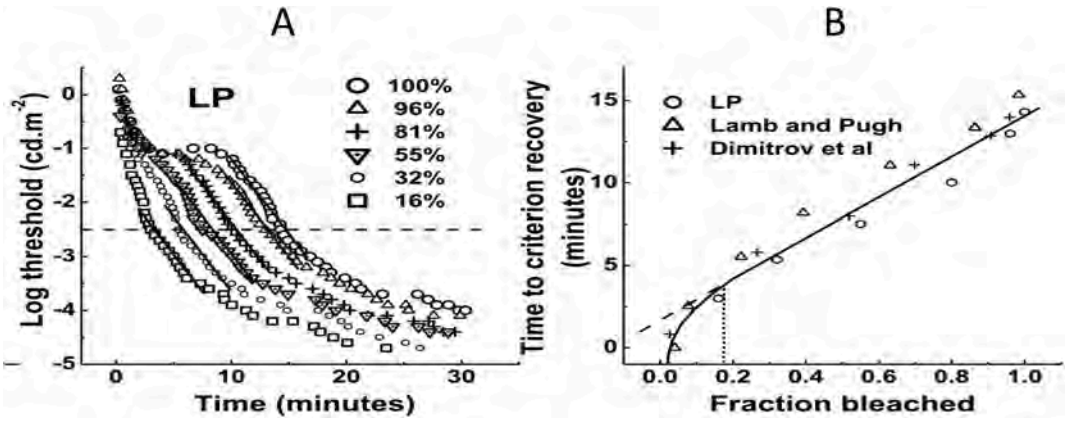

Fig. 6. A) DA curves for a series of different bleach intensities for observer LP. B) Fraction of rhodopsin bleached vs time to reach a criterion recovery of 2.5 log units as depicted by the horizontal dotted line in A. In B the vertical dotted line indicates the fraction bleached above which rate-limited opsin regeneration occurs. As indicated in Fig. 6B, Lamb and Pugh (2004) and Dimitrov et al. (2011) showed similar analyses. From Patryas et al. (2013).

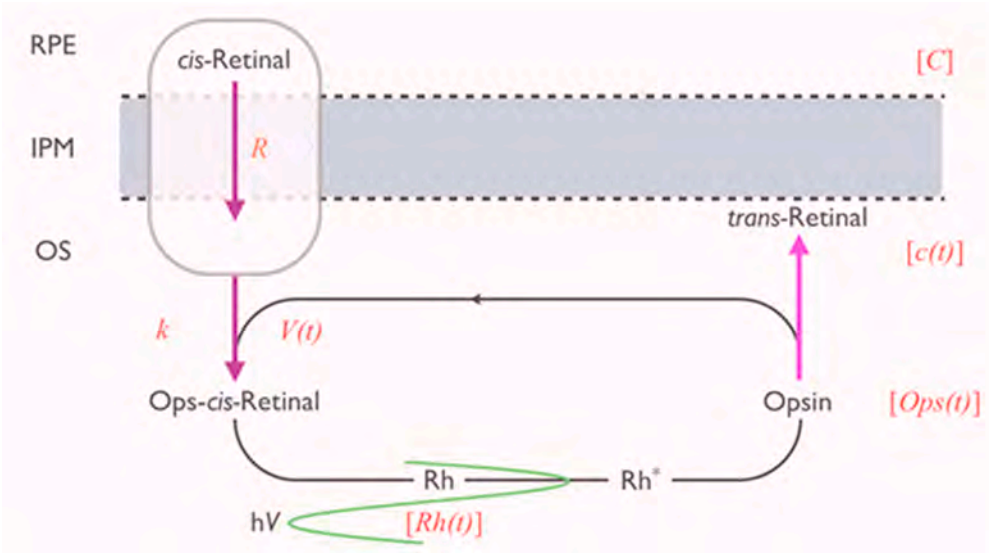

Fig. 7. The resistive barrier version of the MLP model. The regeneration of visual pigment and the removal of photoproduct is rate-limited by the delivery of 11-*cis*-retinal from the RPE to opsin in the outer segment (OS). C - concentration of 11-*cis*-retinal. R – diffusional resistance between RPE and outer segment. *V(t)* - the rate of the binding of 11-*cis*-retinal to opsin (also equivalent to opsin removal and equivalent to pigment regeneration). Rh – rhodopsin. Rh* - meta-rhodopsin. hV- photon. IPM – inter photo-receptor matrix. *Ops(t)* – concentration of opsin. K - bimolecular rate constant for binding of 11-*cis*-retinal to opsin (Kelly (2012) after Lamb and Pugh (2004)).

sensitivity after bleaching in the isolated skate retina. This was compelling evidence that 'free opsin' was inducing the raised thresholds and that sensitivity recovery required the 11-*cis*-retinal to return it to its native rhodopsin.

This did not however establish the link between the *time course* of rate of recovery and the *decay* of R* or the removal of opsin. The correspondence between the timing of rhodopsin regeneration and the psychophysically measured DA curve can be investigated theoretically by taking account of the concentration gradient of 11-*cis*-retinal between RPE and outer segment and the rate at which it binds to form rhodopsin. The theory is the basis for the Mahroo Lamb Pugh (MLP) model, initially formulated by Lamb (1981). Details of the molecular reactions and the corresponding mathematics can be found in Lamb and Pugh (2004). A quantitative mathematical account of the kinetics of sensitivity recovery is briefly described in the next section.

3.11.1. *The Mahroo Lamb Pugh model of opsin removal*

The fundamental idea of the MLP model is that a single factor, the delivery of 11-*cis*-retinal, controls the removal of opsin and thereby the recovery of sensitivity. The model is derived from a series of differential equations based on a simplified retinoid cycle, illustrated in Fig. 7. The starting point in the development of the model is that the difference in concentration of 11-*cis*-retinal in the outer segment and the RPE provide the driving force for delivering 11-*cis*-retinal across a putative resistance barrier, R, between them (but see Lamb et al. (2015a)). Formerly this is stated as follows

$$V(t) = (C - c(t))/R \tag{3}$$

where.

V(t) = rate of bimolecular binding
C = concentration of 11-*cis*-retinal in the RPE
c = concentration of 11-*cis*-retinal in outer segment
R = resistive barrier

This expression has been used in many publications. For example, Rushton and Henry (1968) speculated that the slope of the pigment regeneration function might be used as an estimate of the concentration of 11-*cis*-retinal. The model explains the different kinetics associated with high and low intensity bleaches in that it shows that the level of bleach at which recovery ceases to be governed by first order kinetics is determined by the local concentration of 11-*cis*-retinal. The restriction in the diffusion of 11-*cis*-retinal from the RPE to the opsin in the outer segment, labelled R in Fig. 7, limits the rate of reformation of rhodopsin. A low-intensity bleach only partially depletes the supply of 11-*cis*-retinal in the outer segment so that it reduces c, the concentration of

11-*cis*-retinal in the outer segment, but not sufficiently to be the limiting factor. A higher-intensity bleach causes more depletion of 11-*cis*-retinal which requires transfer of retinoids from the RPE.

Remarkably, the model predicts that the slope of the straight line decay of S2 in a semi-log plot is directly proportional to the concentration, C, of the 11-*cis*-retinal in the RPE but independent of the diffusional resistance, R. Note that this variable, the free concentration of 11-*cis*-retinal, has not been measured chemically. In the case where the slope become zero, this implies that the local concentration of 11-*cis*-retinal is 0. A more recent version of the model favours the idea the rate-limiting step is enzymatic (rather than resistive) but this does not change the kinetics of the process (Lamb et al., 2015b). The main reason for introducing this figure is to emphasize the importance of the underlying kinetics and the fact that they predict the psychophysical data extremely well. Note that, for cones, pigment regeneration can be slower than predicted for high intensity exposures (Mahroo and Lamb, 2012).

4. The dark adaptation curve: methods and analysis

4.1. Methodology for generating the dark adaptation curve

Here we review the phenomenon of DA, the gradual recovery in sensitivity in low lighting following exposure to a bright light (Hecht, 1937). As discussed above, the wide range of luminance over which cones and rods can operate creates a methodological problem for accurate measurements under non-laboratory conditions. When rod function was first investigated in ophthalmic clinics, the Goldman-Weekers device (Haag–Streit, Köniz, Switzerland) was used. It remained in service in clinics for many years and continues to be used, if sparingly, today. The main technical challenge lies in measuring sensitivity to very dim lights in total darkness over a range of 6 log units of intensity over a period of perhaps 20–30 min. The recovery function is highly non-linear with seven parameters and two inflexion points reflecting the transition between three distinct physiological mechanisms with different time courses. It is for this reason that the technique has been regarded as rather cumbersome and unsuited to clinical application. Notwithstanding these challenges, the method of DA has proved extremely valuable in matching the psychophysically observed stages to the underlying physiology. Given the widely accepted association between slowed DA and early AMD, the technique can be expected to be genuinely useful in understanding the different stages of AMD. Note that the typical dynamic range of computer monitors is limited to around 2.5 log units so, in computer-based methods, the dynamic range of the monitor is extended with neutral density (ND) filters, as described below.

4.2. A PC based system

Here we describe a method based on a PC reported by Patryas et al. (2013) and subsequently in Tahir et al. (2017). The set-up is illustrated in Fig. 8, although the earlier work used spots rather than arcuate stimuli. The technique is based on a PC driving a ViSaGe graphics system (Cambridge Research Systems, Rochester UK) and a modified version of the Visual Psychophysics Engine (VPE) software. ND filters were placed in front of the stimuli to extend their dynamic range.

The observer fixated the small (0.3°) red (640 nm) fixation cross and, following the presentation of the bleach, responded to a circular 1° test spot presented at 1 Hz at 11° eccentricity. For the initial period, the

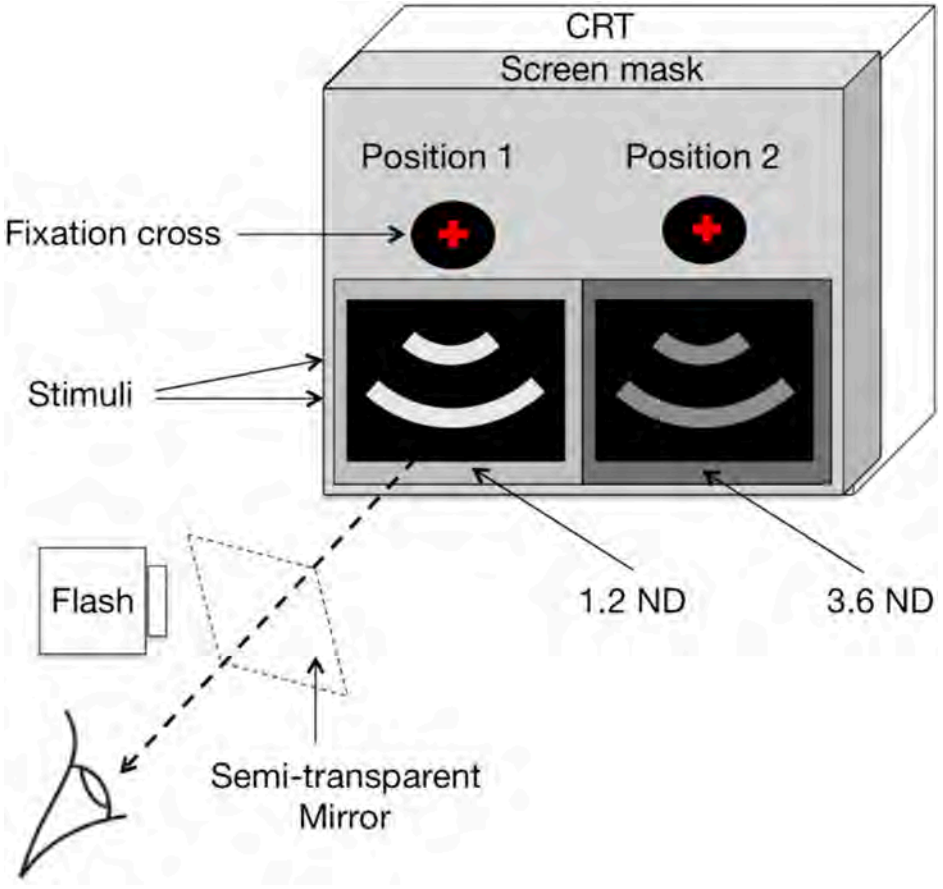

Fig. 8. Dual arc experimental set up. The location of the bleaching light was controlled by the semi-silvered mirror to ensure it matched the retinal position of the stimuli. Measurements were undertaken using position 1 until the stimulus intensity fell below −2.5 Log cd•m^{-2}, at which point fixation and stimuli were moved to position 2 (Tahir et al., 2017).

stimulus was presented in position 1 and was attenuated by a 1.2 log unit ND filter. As sensitivity improved, the stimulus luminance at threshold was reduced to the minimum available luminance. At this point, after around 12 min, the fixation cross and stimulus were switched to position 2 where they were attenuated by an additional 2.4 log unit filter. This transition, not noticed by the observer, gave a total dynamic range of 5.5 log units. A similar approach for extending the dynamic range of a PC monitor was developed simultaneously and described in Dimitrov et al. (2008).

4.3. A dual arc stimulus

A version of the PC-based method was further developed using two arc-shaped stimuli, as illustrated in Fig. 8. These appeared in the inferior visual field at either 3° or 5.5° eccentricity. The inner stimulus was presented first, usually within 20–30 s of the cessation of the bleach. The outer stimulus appeared after 2 s of the observer setting the threshold for the inner stimulus. Stimuli appeared alternately in this way and, when the luminance of the threshold setting reached −2.5 Log cd•m^{-2}, the stimulus and fixation location were switched to position 2 (see Fig. 8). For further details see Tahir et al. (2017).

This configuration was used to investigate reports that the slowing of DA in AMD patients may be spatially heterogeneous. By presenting the targets consecutively, as described below, a pair of DA curves can be generated in one session. Whether or not the well known DA abnormality in older eyes is uniformly distributed across the retina is important when segregating normal from abnormal DA curves. The shape of the stimuli means they correspond to the retinotopic fanning of photoreceptors with eccentricity. An important consideration is that the method generates two curves from exactly the same bleach.

The stimuli were designed to be approximately photopically matched but to compare regions where rod count was substantially different (Fig. 9). The photoreceptor counts are based on donor eye data in Curcio et al. (1990). In the outer stimulus, there are around 2.5 times more rods than cones. The results of the application of the dual arc technique in testing early stage AMD patients are discussed in section 6.

4.4. The application of a long wavelength background

A major consideration when designing a system for assessing DA for clinical trials or in clinics is that the test should be of short duration, sufficiently robust to return valid and repeatable results, comfortable for observers and easy to operate and understand. Here we describe a technique involving the introduction of a long wavelength (655 nm) narrow-band (bandwidth 20 nm) dim background. This can be expected to reduce the duration of the test because it raises the cone threshold and thereby shortens the cone phase of the curve. It is also more comfortable than a totally black background, especially for naïve observers. Rods have very low sensitivity to long-wavelength light, so we might expect that this background would not affect the rod-mediated DA parameters. In particular, applicability of the technique is dependent on the S2 component being independent of the background.

Briefly, the set up was a purpose-built digital device in which it was possible to change the intensity and wavelength of the background. Three different intensities of the red background were compared with a zero background. Eleven normal observers were tested. Measurements were performed on different days and the sequence was randomised.

The results are presented in Fig. 10. It is apparent that the cone

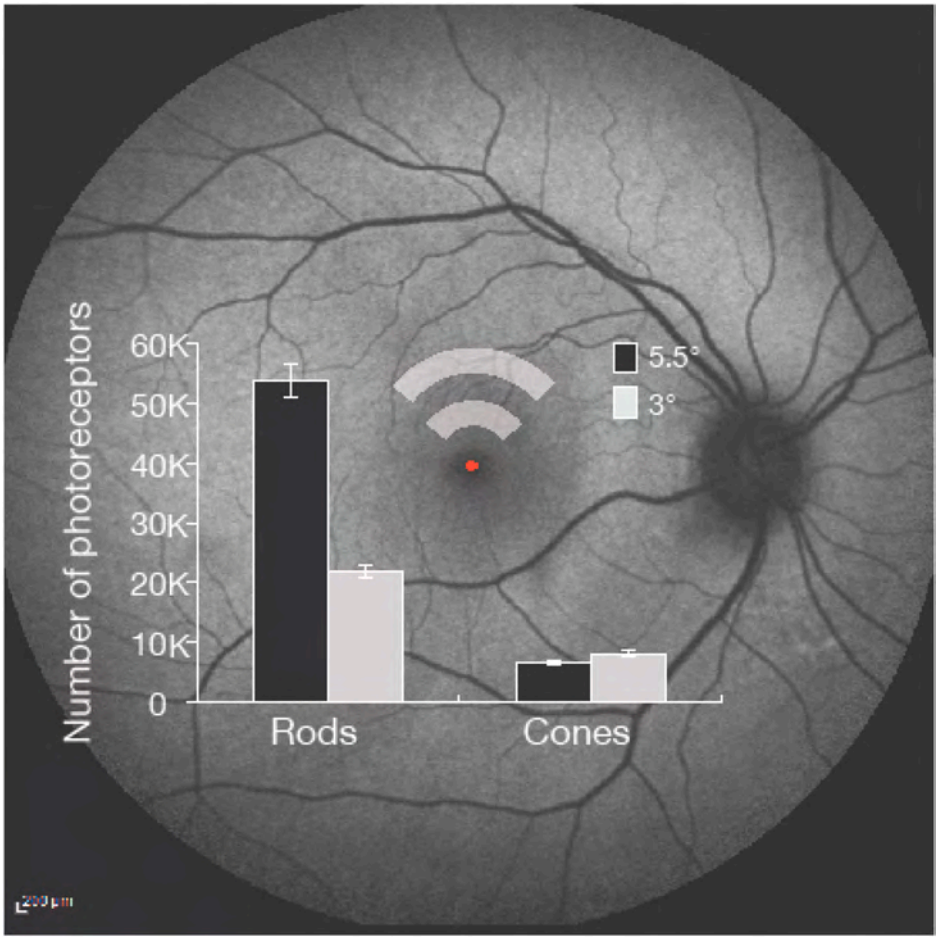

Fig. 9. The location of the dual arc stimuli superimposed on an image of the retina and the relative numbers of cones and rods stimulated. From Tahir et al. (2017).

threshold is systematically controlled by red luminance as expected. The rod-cone break, α, is shortened ($P < 0.001$) compared with the zero background condition. One of the important issues addressed here is whether the slope of S2 would be affected by the red background.

As the rods are virtually blind to the red light and as S2 is exclusively mediated by rods, S2 should be independent of red background luminance. The statistics confirmed that this is the case at the range of luminances used ($P = 0.39$). It can be concluded that, where the primary objective is to determine S2 (as is usual in clinical conditions), a red background of luminance up to 0.2 cd•m^{-2} is likely to return the same value of S2 as a black background.

4.5. The bleaching light

When optimising the test time, it is important that bleach intensity is carefully selected. For reasons outlined above in Section 3.1, the bleach should be greater than around 20% because this then falls in the range where S2 is rate-limited. However, the application of a high-intensity bleach can markedly increase the rod-cone break time, α, as illustrated in Hecht (1937) so, ideally, a customised compromise bleach intensity should be identified so as to maintain as short a test period as possible. This is especially important for older observers who are more likely to experience fatigue and discomfort and thereby produce noisy data when the test time is prolonged. Note that, for longer bleach durations (more than several seconds), calculating bleach parameters will result in a different calculated bleach depending on whether first order regeneration kinetics or the MLP rate-limited model is used.

4.6. Data acquisition; ramp rate

The technique for acquiring the data in the DA method needs to take into account the fact that the threshold is changing systematically with time. Different approaches have been used to cater for this, with the most important factor being that presenting the stimulus at a luminance higher than that of the previous threshold must be avoided because this causes reduction in local sensitivity. One approach is to use a ramping technique in which the stimulus is reduced in luminance by approximately 10 dB immediately after setting a threshold. The stimulus is then gradually increased until the observer detects the target and presses the response button. Judicious choice of the parameters of this procedure is important. If the observer is obliged to make too many responses in a short time, this can cause fatigue.

4.7. Repeatability of the DA method

The reliability and repeatability of the DA technique was systematically investigated in Christoforidis and Zhang (2011). They tested 16 normal observers between 24 and 52 years old. The method used was an analogue instrument, the Goldmann–Weekers dark adaptometer. The standard bleaching of 5 min through dilated pupils was used with a luminance of 2700 cd•m^{-1}. Observers performed the test on two occasions around 2–3 months apart. The authors found no statistically significant learning effects.

Patryas et al. (2013) used the PC based system described above to test 33 normal observers, divided into older (≥45, n = 16) and younger (≤45 n = 17) groups. A localised bleach of between 30 and 98%, depending on pupil size, was used. There was a significant difference for S2 between the groups ($P < 0.001$). Coefficient of variability (CoV) was 15% and coefficient of repeatability (CoR) was 0.07 for S2. From the standard mean *vs* differences plots it was clear there is minimal bias for both old and young eyes.

4.8. Modelling the DA curve: an historical perspective

Assigning parameters to the DA curve is not straightforward. For example, in their study of the link between DA and age, McFarland and Fisher (1955) tested 240 subjects from age 16 to 89 with 30 samples in each decade. Initially they attempted to find an equation that allowed them to identify the transition between cone and rod function (α) for all 240 curves. As there was so much variability they then averaged across age and were able to show strong age effects by plotting the data as two exponential functions. Their approach generated a substantial data set which corresponds to current findings.

Coile and Baker (1992) fitted a single exponential function to their data because they were not concerned with cone thresholds. As they were also interested in the link with pigment regeneration (which they measured simultaneously with the psychophysical thresholds) they were again able to show an age effect. Jackson et al. (1999) fitted a four-linear component model to their data set obtained from 94 observers. This procedure fits two linear components to the cone section of the curve and two linear components to the rod-mediated phase. They also used a non-linear analytical approach that allowed unbiased estimates of the transition times and recovery rates to be obtained. Essentially this involved iteratively solving for the various parameters until a pre-specified stopping point was reached. The method is described in McGwin et al. (1999). Dimitrov et al. (2008) utilised a single exponential decay model applied separately to cones and rods. They assumed the time constant of their second component was equivalent to S2, as described by Lamb (1981).

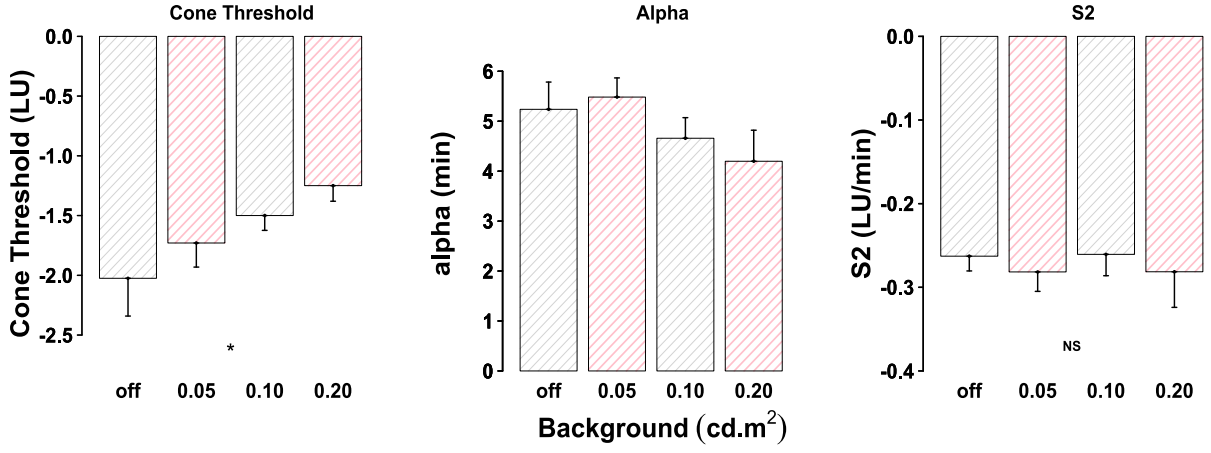

Fig. 10. Three DA parameters as a function of red background intensity compared with zero luminance (Rodrigo-Diaz, 2017). (For interpretation of the references to colour in this figure legend, the reader is referred to the Web version of this article.)

4.9. Managing noise

As described in Kelly (2012), the inherent noise in DA thresholds can be regarded as mathematically random, with three components, namely i) attention lapses, ii) anticipating or guessing a threshold iii) variation in the criterion.

Although these effects are regarded as independent of each other (Treutwein, 1995), this may not always be the case. There are some considerations that are specific to DA curves and the most obvious is that, during the main part of the procedure, the threshold is changing rapidly with time. If sampling is too fast or too slow the data become autocorrelated leading to characteristic zigzagging of the recovery curve. This would adversely affect the accuracy of the estimation of the slope of the recovery function (Kelly, 2012).

A further complication may be the effect of age on these factors, partly because there is a well-established increase in reaction time with age and partly because there are likely to be more so-called lapses in older observers. These effects can be mitigated by optimising the sampling rate of thresholds.

4.10. Characterising DA curves

The DA curve is frequently described in terms of an exponential bilinear function, as in equation (4). The attraction of this approach is that, following Lamb (1981), it is based on the underlying molecular activity that explains the three phases of recovery as described in Section 1.

The 7-parameter version of the model is formally set out below

$$Thresh = \theta_1 + \theta_2.\exp\left(-\frac{t}{\theta_3}\right) + \theta_4.\ h(t,\theta_5) + \theta_6.h(t,\theta_7) \tag{4}$$

where $Thresh = threshold$ and $h(t,\theta_i)$ is a step function whereby

$$h(t,\theta) = \begin{cases} 0, & t-\theta_i \le 0 \\ t-\theta_i, & t-\theta_i > 0 \end{cases} i \in (5,7)$$

the 7 parameters are defined in Table 1;

4.10.1. A five-parameter version of the model

The above equation and Fig. 5 describe the performance of a young healthy observer. However as discussed above there are circumstances where it is convenient for the recovery function to be composed of 5 parameters. In these cases a satisfactory fit to the data can be achieved by applying an exponential and a single linear region representing S2. An obvious example is the case where the observer's recovery is slowed, as occurs in many older eyes or in pathological cases. In this case the final 2 parameters of β and S3 would be regarded as superfluous. The 5-parameter model is described below.

The decision as to which model is most appropriate can be formalised using the Akaike Information Criterion (AIC) described in Akaike (1974). The technique avoids hypothesis testing and *p* values but compares the merits of one or other model on the basis of index of information lost.

Table 1
Parameters of the MLP model.

Description	θ	Units
Cone threshold	θ_1	(cd•m $^{-2}$ scot)
Exponential coefficient	θ_2	Log_{10} (cd•m scot)
Cone time constant	θ_3	minutes
Slope of S2	θ_4	Log_{10} (cd•m $^{-2}$ scot)•min^{-1}
Rod cone break α	θ_5	minutes
Slope of S3	θ_6	Log_{10} (cd•m $^{-2}$ scot)•min^{-1}
Rod-rod break β	θ_7	minutes

4.11. The least squares method

Characterising non-linear multicomponent models, as described above, is complex because it is necessary to solve for many interdependent parameters simultaneously. The conventional approach has been to use the least squares method, minimising the vertical distance between the data points and the model (the residuals), by varying the particular parameter, θ, according to a response function or loss function, as follows

$$L(\theta) = \sum_{i=n}^{n}\left(Thresh_i^* - Thresh(ti,\theta)\right)^2 \tag{5}$$

where *n* is the number of observations, $Thresh_i^* = i$th threshold at time *ti* and *Thresh(ti,θ)* is the model estimate using parameter *θ* at time *ti*. Essentially this is a maximum likelihood procedure in that the parameter estimates are optimal when *L(θ)* is the global minimum (Bates and Watts, 1988).

4.12. Finding the optimal parameters to describe the data

Minimising L*(θ)* can be achieved in two ways. The first is an analytical approach in which the partial derivatives of the loss function are used to find a path of maximum descent. This raises the technical difficulty that equation (4) contains step functions between the different stages of the function. There are two step functions in the 7-parameter version, the first between the cone stage and S2 and the second between S2 and S3. Solving this equation is not straightforward because step functions are difficult to differentiate.

Alternatively a technique known as the Direct Search method can be used, in which the test estimates are compared under a series of rules. This optimization technique was first described by Nelder and Mead (1965). See Kelly (2012) for a discussion of the relative merits of these techniques. Note that the Nelder Mead method is implemented as the Solver Tool in Microsoft Excel.

Nelder Mead is robust when used on noisy or discontinuous data and is largely independent of whether or not there are first and second derivatives of *L(θ)*. In this sense it is appropriate for characterising DA data; the algorithm performs a succession of transformations in order to find a minimum for the global variable *L(θ),* with the end point being reached when a number of iterations has been completed or when changes in *L(θ)* are minimal for further transformations. Typically, nonsensical results can be avoided using a so-called multi-start algorithm. The main limitation of this approach is that it is necessary to analyse the data retrospectively and this in turn increases the time before the results of the test can be presented. Furthermore the process is rather cumbersome if a large number of curves are to be analysed.

4.12.1. Replacing the discontinuous step with a switch function

Apart from making the differentiation of the function technically difficult, using the step function in the model is time-consuming and computationally expensive. Instead, a logistic switch function of the form shown below can replace the step function. Essentially *h()* in equation (4) is replaced by the function H. A generic version of the function is

$$H(\rho,x) = \frac{x-\rho}{1+\exp(-k(x-\rho))} \tag{6}$$

where k = slope factor.

ρ = transition time
x = response time

Heuristically k = 40 was chosen. See Appendix C.

4.13. Extraction of the parameters; background mathematics

Here an analytic technique for determining the parameters of a 5-parameter DA curve is described. For the purposes of the analysis, equation (4) can be re-stated in 5-parameter form as in equation (7). In this form, rod contribution is zero before α, and additive after α;

$$Thresh = CT + CC * \left(exp\frac{-t}{\tau}\right) + \frac{S2*(t-\alpha)}{1+\exp(-k*(t-\alpha))} \quad (7)$$

where *Thresh* = threshold.

CT = cone threshold
CC = cone offset at t = 0
t = time
tau = cone time constant
S2 = Slope of S2
k = a parameter controlling the rate of switch transition (see Appendix).

When the above switch is included, the analysis is hundreds of times faster than with the step function and this applies especially when data are noisy, as is frequently the case with naïve observers.

The sum of least squares, or loss function can therefore be written as

$$L\left(\widehat{\theta}\right) = \sum_{i=1}^{n}\left(\text{Threshold} - \text{Thresh}\left(\widehat{\theta}, t_i\right)\right)^2 \quad (8)$$

where. $Thresh(\widehat{\theta}, t) = \theta_1 + \theta_2 \exp\left(\frac{-t}{\theta_3}\right) + \theta_4 \frac{(t-\theta_5)}{1+k*\exp(t-\theta_5)}$

And $Thresh\ \widehat{\theta}, t$ = estimated threshold at time t.

θ_1 = estimated cone threshold
θ_2 = estimated cone exponential coefficient
θ_3 = estimated cone time constant
θ_4 = estimated S2
t = time
θ_5 = estimated α
k = a parameter controlling the rate of switch in the transition between cone threshold and S2.

In order to find an estimate of the parameters $(\widehat{\theta})$ of the model, a sequence of n threshold measurements over time is collected and the difference between the actual measurements and estimated values for a given set of parameters is calculated. These differences are squared and summed, then the parameters of the model are iteratively modified until the sum of squares is at a minimum.

4.14. Plain Gradient Descent

The gradient of the loss function (equation (5)) can be used to locate the minimum. This can be achieved in a number of ways, collectively called Gradient Descent methods. In brief, the initial gradient, $\widehat{\theta}_1$, of the loss function for a set of parameters is determined. This is the first of a sequence of values for the gradient. Recall that each $\widehat{\theta}$ represents a vector of 5 parameters. These values are then used to make a further estimate, $\widehat{\theta}_2$, and a new gradient is found corresponding to a new set of parameters, so that $\widehat{\theta}_1$, $\widehat{\theta}_2$, $\widehat{\theta}_3$ …. $\widehat{\theta}_n$ approach the optimal value. This procedure is repeated until further changes yield no improvement in the value of $L\widehat{\theta}_n$.

Formally the method is written as follows;

$$\widehat{\theta}_{n+1} = \widehat{\theta}_n - \eta\nabla_{\widehat{\theta}}L\left(\widehat{\theta}_n\right) \quad (9)$$

where …

$\widehat{\theta}_{n+1}$ = next consecutive estimate
$\widehat{\theta}_n$ = nth estimate
η = step size
$\nabla_{\widehat{\theta}}L(\widehat{\theta})$ = slope of the objective function at the parameter estimate $\widehat{\theta}$

4.15. A novel real-time technique for fast parameterisation of DA curves

The theoretical framework described above has been implemented in R and in Python. Using the method, the model parameters and their corresponding standard errors can be obtained within 800 ms.

This means that the optimised model parameters and their errors can be updated between threshold settings and presented as part of a graphical readout. The fast implementation means that data collection can be terminated as soon as the confidence intervals reach acceptable values. The values returned by this technique are the same as a Monte Carlo (iterative) method but many times faster.

5. Age related changes in outer retinal structures and their impact on DA

It has been known for many years that DA is less efficient as the eye increases in age. Here we discuss the physiological changes associated with this effect. There is a delicate, mutually beneficial, relationship between the outer retinal cells, (photoreceptors, RPE and Muller cells) and the outer ocular structures (Bruch's membrane, the choriocapillaris and the choroid). All undergo systematic structural changes throughout life: rods are lost, Bruch's membrane thickens and the choroid thins. There is a fine line between normal aging and pathological change, which is particularly exemplified in early AMD. Whilst there is overlap between changes due to age and those to disease processes, aging is often defined as occurring continuously from youth to old age in the majority of individuals without overt clinical consequences. This usually refers to morphological or functional changes; these are difficult to define without testing large numbers of cases and identifying a criterion either side of which might be regarded as normal or abnormal. As not everyone develops AMD, it is important to ask how some individuals find a balance between the inevitable age-related changes and overt pathological phenotypes that signal the onset of the disease. The main functional change in AMD is slowed sensitivity recovery, manifest in the DA curve, so it is important to assess the normal physiological changes that occur with age in the context of this phenomenon.

5.1. Rods may be selectively vulnerable in aging and AMD

It has long been assumed that, as the eye ages, there is a preferential loss of rods compared with cones. As discussed below, there are reports of an age-related deterioration in cone function with age and certainly cone function has been reported as abnormal in AMD. Estimates of the extent of rod vulnerability vary but it is agreed that, from 30 to 90 years old, rod numbers decrease by around 30% (Curcio et al., 1993). This was confirmed in a separate study by Panda-Jonas et al. (1995). Note that rod-specific vulnerability is not spatially homogenous but occurs most conspicuously in the parafovea, up to around 2–3 mm from the fovea, thereby occupying an annulus of between 4° and 7°. As rod numbers decline, surviving rods expand to fill the vacated spaces. Cones remain and appear unchanged. Curcio (2001) reported that this also applies to non-exudative early AMD and that, whilst the changes are histologically qualitatively similar in the aging retina, the spatial distribution in normal aging appears to be different from that in early AMD. In a seminal paper, Curcio et al. (2000) proposed that these phenomena are linked to changes in Bruch's membrane, suggesting that its ability to transfer important nutrients and retinoids between the choriocapillaris and the rod outer segments is impeded.

5.2. Retinal pigment epithelium

From around 40 to 80 years of age, the numbers of RPE cells fall from around 4000 to 2000 cells·mm^{-2}, there are changes in pigmentation and a fall in the number of melanosomes. See Strauss (2005) for a review. These age-dependent changes lead to the proportionate increase in the activity of the surviving cells and may or may not have a functional impact on the RPE as a whole and in particular on rods. It has also been suggested that intracellular congestion by lipofuscin may impede one of the many RPE roles, including phagocytosis (Dorey et al., 1989).

5.3. Disposal and renewal of outer segments

Photoreceptors accumulate photo-damaged proteins and lipids because they are exposed to high intensity light. The concentration of phototoxic substances therefore accumulates throughout the day (Bok, 1993). In this carefully orchestrated process, the outer segment is newly rebuilt from its base at the cilium. The tips of the outer segments containing the highest concentration of toxic products are removed through phagocytosis by RPE cells. This mechanism maintains constant photoreceptor length. It is under diurnal control and is a further example of the interdependence between photoreceptors and RPE. The turnover rate for a complete outer segment is around 10 days (Marshall et al., 1979). The onset of light is said to be the major trigger for a burst of outer segment shedding (Besharse et al., 1977).

5.4. Bruch's membrane

The physiology, molecular composition and structure of Bruch's Membrane changes dramatically with age. Its filtration capacity is impaired and there is an overall increase in thickness which is largely linear and linked to calcification. The increase in volume is thought to be mainly due to oxidised waste products of RPE metabolism. Inevitably, thickening leads to loss of elasticity and reduced hydraulic permeability. For a review see Booij et al. (2010).

The accumulation of lipids in Bruch's Membrane is especially evident in the macular region (Sheraidah et al., 1993). With time, lipid inclusions accumulate in the elastic layer and form a lipid wall (Guymer et al., 1999). Historically, lipids have always been thought of as the primary component of drusen; the deposition of lipids in Bruch's Membrane provides an obvious link with AMD (Steinmetz et al., 1993).

5.5. Choroid and choriocapillaris

The choroid and choriocapillaris become thinner as they age so that, in the sixth decade, they are less than half the thickness found in youth. In addition, the size of the choriocapillaris lumen is reduced by a third (Ramrattan et al., 1994), making the vessels liable to occlusion by red blood cells. Overall, with advancing age, blood flow is reduced and oxygen tension, metabolite delivery, waste clearance and temperature regulation are all compromised (Chirco et al., 2017).

5.6. Selective reduction of rod-based function in the normal older eye

Rod-specific loss was shown in studies of donor eyes (Curcio et al., 1993) and reduced scotopic vision in older eyes was also established. For example, Sturr et al. (1997) found 0.39 log unit higher scotopic thresholds in older (mean age 72.6) than younger (mean age 24.1) observers. Jackson et al. (1998) reported a 0.5 log unit reduction in scotopic sensitivity in healthy normal older observers after taking account of lens optical density and pupil size.

These observations raised the possibility that they might be accompanied by a corresponding loss of function in the *recovery* characteristics of scotopic vision. As noted, there is a 30% loss of rods in the macular region, particularly at around 3.5–10° from fixation (Curcio et al., 1993). The sensitivity loss does not correspond spatially to the reduction in numbers of rods with age. According to Plantner et al. (1991), there is minimal change in the overall levels of rhodopsin across the life span. In general, static scotopic sensitivity loss is not correlated with DA changes and delayed sensitivity recovery is quite often seen when sensitivity loss is normal. It would appear that the dynamic changes are more susceptible to pathological changes, suggesting that the two manifestations of scotopic abnormalities represent different mechanisms, as fully discussed in Curcio et al. (2000).

Post-bleach recovery of sensitivity as a function of age in healthy adults was investigated systematically by Jackson et al. (1999). Studying 94 adults ranging in age from the 20s to the 80s, they showed a marked reduction with age in the rate of rod-specific sensitivity recovery. They controlled for pupil size and ocular media changes and were therefore able to attribute their effects to impairment in the regeneration of rhodopsin. There was an increase of 39 s·decade^{-1} in the time to the rod-cone break, α, and the slope of the second phase of the rod-mediated part of the curve decreased by 0.02 log units^{-1}•min-^{1}•decade^{-1}. Note that 21 subjects had large drusen, focal hyperpigmentation or both. A separate analysis showed that these did not contribute to the relatively high decade-by-decade age effect on the rod-mediated phase of DA, indicating that the effect is due to biological aging rather than early AMD. Owsley et al. (2014) investigated the association between rod-mediated DA and risk factors for AMD in 381 older healthy participants with normal maculae. They reported that 25% of these had slowed DA and that this characteristic was associated with risk factors for AMD. The study exemplifies the problem of separating abnormal DA due to age from that attributable to early AMD.

Patryas et al. (2013) investigated the age effect using the PC-based technique described above to test DA in an older group (≥45 years, N = 16) and a younger group (≤45 years, n = 17). The main aim of the experiments was to compare the variability in the different parameters. The values for S2 were comparable with previous studies: S2 for the younger group was 0.23 ± 0.03 cd•m^{-2}•min^{-1} and 0.19 ± 0.03 cd•m^{-2}•min^{-1} for the older group ($P < 0.0003$). The data are presented in Fig. 11. The cone-rod break, α, and T_{30} were not statistically different between the two groups and S3 was slightly different in the two groups. Repeatability was formally tested and, for S2, CoV = 15% and CoR of 0.07 was reported.

There is no doubt that, under controlled conditions and despite the different bleaches due to pupil size, the method can reliably detect small changes in S2 in a relatively small population. If senile miosis effects

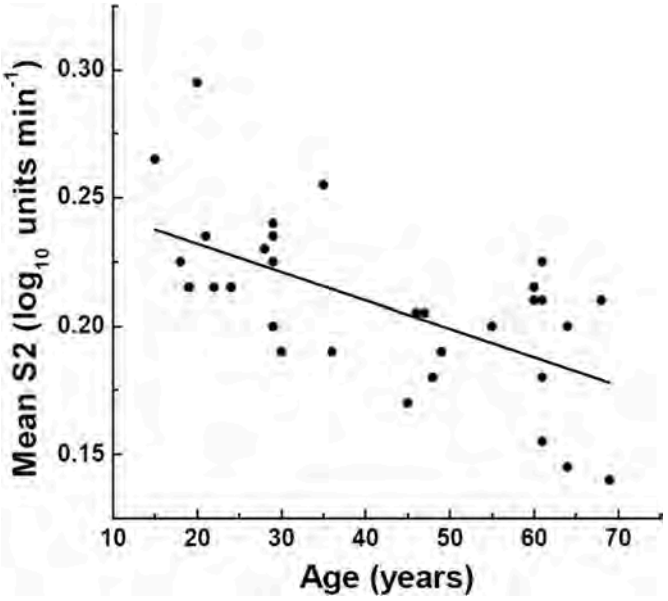

Fig. 11. S2 vs age based on 2 measurements (Patryas et al., 2013).

were taken into account this would increase the age-related change in rod recovery. This study did not compensate for changes in scotopic spatial summation. Nevertheless in this particular study, the power to detect a difference between old and young eyes was 0.96.

5.7. Investigation of the age effect using the dual-arc set up

Many of the phenomena discussed above are studied because they may help to tease apart biological aging from pathological effects such as those seen in AMD. DA and S2 in particular are changed in similar ways both in aging and in early AMD. Thus, identifying differences between the two groups depends on testing large groups of individuals. An alternative is to discriminate patients and normals by measuring two locations in a single observer and in a single session.

The AMD deficit is most severe in the parafoveal region, suggesting that localised abnormalities may be an early sign of AMD. Recall that Curcio et al. (1993) showed sharp reductions in the number of rods in a ring shaped region between 3° and 9° around the fovea in AMD. As described in Section 4, by stimulating slightly different regions of the retina, the dual arc technique established that the parameters of the DA curve were modified in specific ways.

The data in Fig. 12 show the DA curves obtained using the arc shaped stimuli. S2 is markedly steeper for the peripheral outer stimulus and this effect is highly statistically significant ($P < 0.001$) as might be expected given that 2.5x more rods were activated by the outer than the inner stimulus. Of interest is the fact that there were minimal differences in α or β when the data were grouped in this way.

In order to understand the relative effects of age on the location effect seen in Fig. 12, the results of an older and younger group were analysed in a multivariate ANOVA. There was a strong effect of location ($P < 0.001$) and slightly weaker effect of age ($P = 0.037$) and no location*Interaction effect. Post hoc analysis on location showed a strong effect for both groups for S2. Location effects were slightly stronger in the older group for α and β. In order to use these effects as a template for how a particular parameter, say S2, changed in the normal older eye, we would be most interested in the *difference* between parameters obtained from inner and outer stimuli. The data from this analysis are reproduced in Fig. 13. Where effects reach statistical significance, thick lines are drawn between the panels. Crucially these differences are about the same for older and young groups.

For S2, there was a difference of 0.03 log scotopic cd•m $^{-2}$ between the outer and inner stimuli for both groups of observers. This suggests that the slowing of S2 with age is relatively uniform in a small region of the retina encompassing the parafovea. It is this region that has been reported as showing regional abnormalities in scotopic sensitivity in AMD (Owsley et al., 2000). Dimitrov et al. (2011) reported similar effects to those above by measuring rod sensitivity recovery. They found faster recovery in normals than patients for a 2° diameter stimulus and this was more marked at an eccentricity of 10° than at 3.5°.

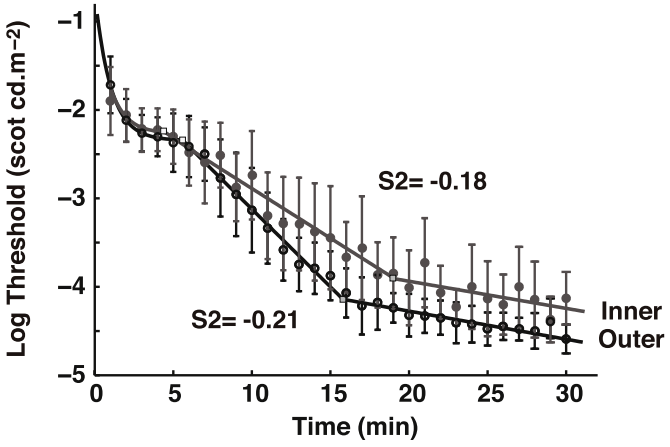

Fig. 12. DA curves obtained from the two arc stimuli in 30 normal individuals. One minute binwidths are used for clarity. The inner and outer arcs are matched in terms of the numbers of cones activated. The outer stimulus activates 2.5x more rods than the inner. This explains the steeper slope of S2. Error bars = SD.

6. What the DA curve tells us about AMD

The following sections discuss the extent to which measures of photopic and scotopic vision can be linked to the morphological abnormalities in the early, non-neovascular stages of AMD. Although there are technical challenges, functional assessment of disease has many benefits. Identifying an aspect of visual function that can accurately detect, grade and monitor disease progression will be particularly valuable as new therapies and management strategies emerge.

6.1. Defining AMD

Age-Related Macular Degeneration (AMD) is a major cause of blindness in older people in the developed world, as reported by Wong et al. (2014) and Bressler et al. (2003). A subtle, little understood, combination of genetic and environmental factors contribute to disease development. Around 10–15% of cases are affected by the 'wet' form of the condition in which there is a substantial loss of central vision due to exudative changes in the outer retina (Bhutto and Lutty, 2012).

According to Klein et al. (2007), the 15-year cumulative incidence of dry AMD based on colour fundus photographs of patients between 43 and 86 was 15%. From the analysis of these and other authors it is estimated that around 5–10% of patients progress to severe disease after 10 years. By far the majority of those suffering from AMD, around 23% of those over 75 according Klein et al. (1992), have early dry AMD. Although progressive, the pattern and rate of development in dry AMD is notoriously variable. Patients may have minimal visual disturbance over many years and be aware only of slightly impaired vision under low lighting.

Drusen are the defining feature of non-neovascular AMD, so how they are identified, graded and classified has a substantial impact on models of their formation and clinical significance. There is a wide spectrum of drusen types, usually characterised in terms of ultrastructure and morphology. As they are usually the precursor to more severe forms of AMD, understanding and staging their development and clearance cycles is crucial. The possibility of interrupting the transformation from benign early stage to severe sight loss rests on the formation of effective management strategies. As there is a clear biological link between the excess accumulation of lipids and the formation of large soft drusen, it has been suggested (Curcio, 2018) that later stages might be prevented by an appropriate pharmaceutical intervention in a similar way to how statins have been used to manage the accumulation of cholesterol systemically.

The biogenesis of drusen should be interpreted in light of the changes seen in Bruch's membrane. The delicate tissue layers and adjoining space where the accumulation of debris occurs can be seen in Fig. 14, which illustrates the RPE-Bruch's membrane-choriocapillaris complex. The strict anatomical description of Bruch's membrane is of a five-layered structure but the picture can be simplified by omitting the RPE and Choriocapillaris basal layers (Curcio, 2018). The focal deposits called drusen are located between the RPE basal layer and the inner collagenous layer of Bruch's membrane (see Fig. 14). The pathological changes to Bruch's membrane are well documented as cross-linking, thickening and lipidization (Curcio, 2018).

6.2. The classification problem

As illustrated in Fig. 14, drusen are located between the RPE basal layer and the inner collagenous layer of Bruch's membrane. Hard drusen

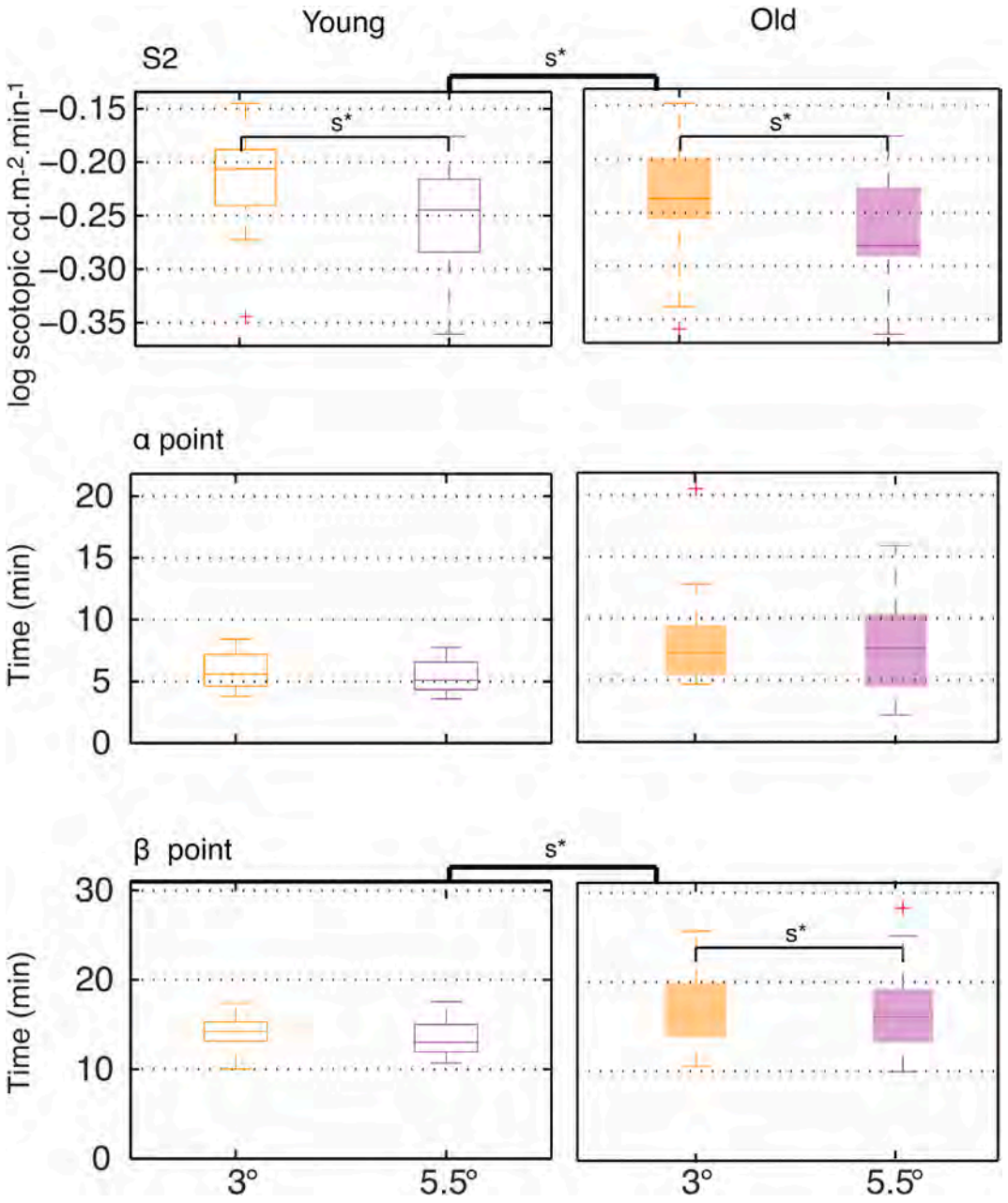

Fig. 13. Box plots of the three parameters for the young (left panel, open squares) and older (right panel, filled squares) groups for inner and outer stimuli. Central line is the median and the edges of the box are the interquartile range. Whiskers extend to the most extreme data points and outliers are plotted individually as + signs. Comparisons between testing location (indicated by a thin horizontal line) or between subject groups (thick horizontal line) are marked s* if statistically significant (Tahir et al., 2018).

are steep-sided, usually small (<63 μm) and electron dense, containing dense hyalinised content. Soft drusen are yellowish white elevations with indistinct borders owing to their sloping sides. A major component is lipoprotein material, as discussed in detail in Curcio (2018).

Some form of universal, evidence-based, classification is important. Many systems of staging of AMD severity based on fundus photographs have been published (e.g. Bird et al., 1995; Ferris et al., 2013). The Ferris et al. study was based on the views of a working committee of experts. They aimed to establish consistency of terminology on relative risk of drusen and pigmentary changes for the development of severe sight threatening AMD. The group set out to distinguish normal retinae from aging-only changes and from those related to AMD using clinical observations. The recommendation of the group are presented in Table 2 below.

The committee recognised that their system should be regarded as a work in progress because technical developments may in retrospect render some risk estimates invalid. A good example of this is the emergence of what are now referred to as Subretinal Drusenoid Deposits (SDD; discussed below) but which may in the past have been misclassified as soft drusen. In fact these were recognised and labelled as reticular drusen in Ferris et al. (2013) but their appearance is slightly ambiguous. As indicated in Curcio (2018), SDD are biologically distinct from drusen and should not be regarded simply as drusen in the wrong place. One final point about classification concerns the importance of disease in the fellow eye. Ferris et al. (2005) devised a simplified points-based severity score and this was followed by Ferris et al. (2013) who reported the results of a survey bringing together a wide spectrum of clinical expertise (see Fig. 15). It was emphasized that, whilst

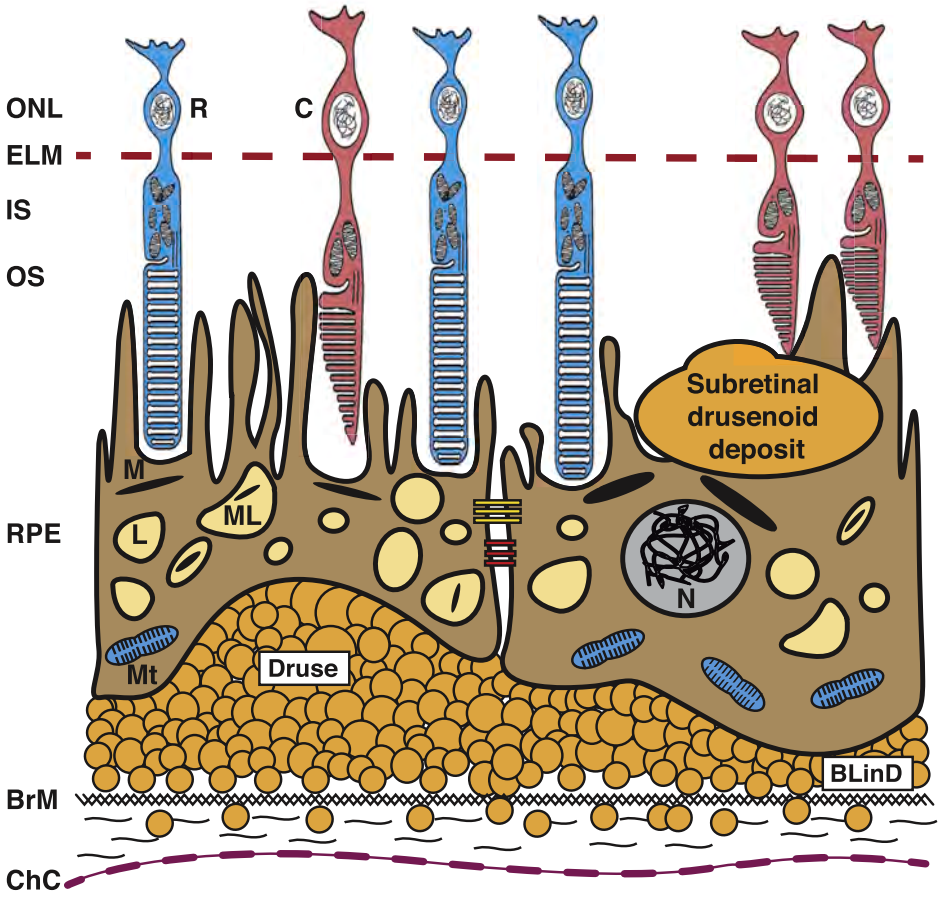

Fig. 14. Soft drusen and basal linear deposits (BLind) are differently formed shapes of the same drusenoid material specific to early AMD. Subretinal drusenoid deposits are located in the subretinal space between photoreceptors and the RPE. RPE cells contain melanin (M), melanolipofuscin (ML), Lipofuscin (L) and mitochondria (Mt). C-cones, R-rod, BrM-Bruch's membrane, RPE retinal pigment epithelium, ChC choriocapillaris. Adapted from Curcio (2018).

recognising the importance of large drusen and pigmentary changes, the bilateral appearance of one or both of these changes resulted in a doubling of the risk score. That is, the grading system allocates a risk score of 1 to each risk factor and to each eye so there is a maximum of 2 per eye or 4 per patient. Hence the 5-year risk for advanced disease is quite low for scores of 0 (no risk factors). The risk doubles (from 12% to 25%) between scores of 2 and 3 and from 25% to 50% between scores of 3 and 4. Similar observations about the need for improvements in the classification system can be found in Spaide et al. (2018).

Table 2
Proposed AMD classification from Ferris et al. (2013).

Classification	Definition (assessed within 2 disc diameters of fovea)
1 (no aging changes)	No presence of drusen or questionable with small size <63 μm, no pigmentary changes (hypo or hyper pigmentation) and no GA
2 (Normal aging changes)	5 to 15 Small drusen (<63 μm), with no pigmentary changes and no GA
3 (Early AMD)	Medium drusen (>63 μm) and ≤125 μm) consistent and No pigmentary changes/GA
4 (Intermediate drusen)	Large drusen (<125 μm) and pigmentary changes no GA
5 (Late AMD)	AMD pigmentary changes. Neovascular AMD Any GA

GA = geographic atrophy.
AMD = age-related macular degeneration.

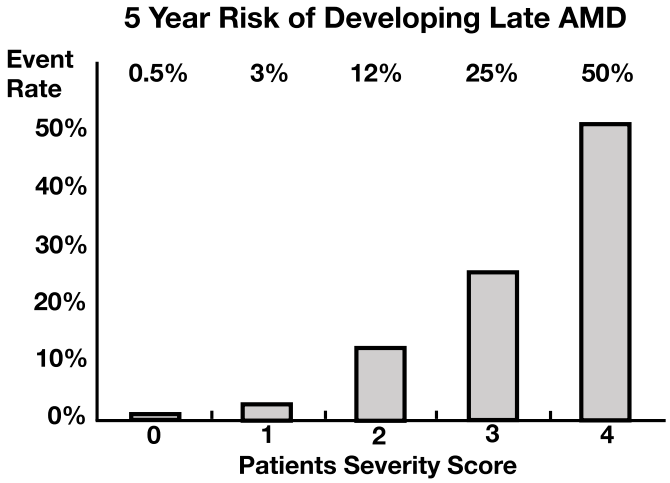

Fig. 15. The link between patient AMD severity scale and the 5 year risk of developing severe AMD. Re-drawn from Ferris et al. (2013).

6.2.1. *Soft drusen and BLinD*

Dry AMD is intensely investigated because it is thought that understanding its development is the route to identifying and managing those who are most at risk of debilitating sight loss. The condition is characterised not by its effects on vision but by the type and number of drusen (Bird et al., 1995). Two types of these extracellular deposits have been described: soft drusen/basal linear deposits (BLinD) and subretinal

drusenoid deposits (SDD). An understanding of how these deposits form and their impact on the physiological processes of the outer retina is essential for identifying new therapeutic and management strategies.

Soft drusen and BlinD have been described as two forms of lipid-rich material that are located in the extracellular space between Bruch's Membrane and the RPE, illustrated in Fig. 14. They are composed mainly of lipoprotein particles secreted by the RPE and as such have been described as an 'oil spill' in Bruch's membrane (Curcio, 2018). They probably originate from dietary fatty acids and remnants from photoreceptor outer segments. They may be misinterpreted as thickening of Bruch's membrane when in fact they are new layers.

It is thought that understanding the pathway for the formation and clearing of drusen may help identify pharmacological solutions for delaying the development to severe sight loss and the late stages of the disease. There are indications that drusen are controlled by regulated mechanisms in that they grow, coalesce and may spontaneously disappear (Curcio, 2018). Although there are similarities to atherosclerosis, the evidence that AMD might be controlled by anti-cholesterol medication is unconvincing. There is a possibility that at least some of the lipids found in Bruch's membrane are derived from plasma and therefore directly from the diet. There is little doubt that transport across this tissue is impeded due to accumulation of lipids, as shown in Bruch's membrane explant studies (Hussain et al., 2010). Various strategies for removing drusen based on 'Skimmers and Dispersant' are discussed in (Curcio, 2018).

6.2.2. Subretinal drusenoid deposits (SDD)

SDD are aggregations of reflective material located above the RPE/Bruch's membrane band (Spaide et al., 2018). They are strong independent risk factors for advanced disease (Pumariega et al., 2011). They have some proteins in common with conventional drusen but differ in lipid content (Rudolf et al., 2008). They were referred to as reticular pseudodrusen by Arnold and Heriot (2007) but have now been reclassified as SDD because of their location and composition. Due to their relatively recent recognition they are not included in any of the large longitudinal trials, but see Ferris et al. (2013). As observed recently by Spaide et al. (2018), much of the thinking about the biogenesis of conventional drusen and SDD has been revised and this may be because SDD are most easily identified using ocular coherence tomography (OCT) rather than colour fundus photographs. In OCT images, a characteristic range of depositions is seen from diffuse accumulations to distinct mound-like deposits (Fig. 1 in Spaide et al., 2018). Note that there are some indications that SDD may represent a different pathological process from soft drusen. Further, the LEAD study demonstrated that Subthreshold Nanosecond Laser Intervention (SNL) slowed progression of the disease but only in patients without co-existing SDD (Guymer et al., 2019). In a cohort study comparing 64 eyes treated with SNL with 77 untreated eyes, a reduction ($P < 0.001$) in area and amount of drusen was reported (Chichan et al., 2021). Although there was an improvement in macular morphology there was no significant difference in visual acuity between the two groups. As discussed extensively in this document, it is important that any assessment of therapeutic measures should include cone and rod based functional measures.

6.3. Abnormalities in DA and AMD

There follows a brief, non-exhaustive, summary of the techniques, collectively called Dark Adaptation, that are designed to assess sensitivity recovery after a bleach in AMD. Curcio et al. (2000) have argued strongly that rods are disproportionately damaged in AMD (Jackson et al., 2002; Owsley et al., 2000). The case is made on the basis of selective rod loss seen in photoreceptor counts in whole mount retinas from donor eyes and the fact that scotopic sensitivity would appear to be disproportionality compromised in DA studies. It has long been known that measuring dynamic aspects of scotopic vision is a particular sensitive index of the integrity of the retinal pigment epithelium/Bruch's membrane/choriocapillaris (Brown et al., 1986; Curcio et al., 1996; Steinmetz et al., 1993). From the early days of investigating these effects, a substantial body of literature has accumulated around the idea that DA can be used to evaluate and perhaps understand the different stages of early and intermediate AMD. Whilst most emphasis is on scotopic recovery, the recovery of cone function after a bleach has also been investigated and there is clear evidence of cone abnormalities, as discussed in Section 6.2.3. Whether or not DA-based methods are effective in assessing AMD is comprehensively discussed in Higgins et al. (2021b).

As discussed above, assessing rate of adaptation is achieved by exposing the eye to a bleach and subsequently measuring visual thresholds to a peripherally presented stimulus in total darkness. The development of the underlying physiology and associated psychophysical techniques has been reported extensively for many years (see Reuter 2011) for a comprehensive review), many of the early studies of AMD using a method based on a modified Humphrey Visual Field Perimeter (Carl Zeiss Meditec Inc, Dublin, CA). These techniques have been further developed and a purpose-built device is now available. This instrument, called the AdaptDx (MacuLogix, Hummeston, PA, USA) has been extensively used in trials of early AMD and some of these are discussed below.

6.3.1. The Rod Intercept Time (RIT)

The AdaptDx is a purpose built instrument for assessing DA in AMD. It employs the technique of Rod Intercept Time (RIT), defined as the time to recover to a criterion sensitivity (usually 4 log units) after the delivery of a bleaching light. The attraction of the approach is its simplicity: it returns a single number as a measure of rod-recovery time. A short-duration version of the method was described by Jackson and Edwards (2008). In this study, a small number of observers ($n = 17$) and AMD patients ($n = 17$) were defined as normal if the RIT was <12.5 min. The cases where AMD was classed as 'intermediate', that is the more advanced of the cohort, were unable to complete the test within the total 20 min testing time. In general AdaptDx data are not subject to fitting with a biological model. The only exception to this is Clark et al. (2011) who compared the slopes of the second and third DA components with retinal thickness.

The idea behind the RIT was to concentrate exclusively on rod-mediated function and reduce the time for the testing. In Owsley et al. (2007), the AdaptDx was used to measure both rod and cone recovery function with a 1.7° circular test spot located at 12° in the inferior visual field. Cone function was measured with a 650 nm light and rod function with a 500 nm light. A 98% bleach was used before the test. Thresholds were evaluated using a 3-down 1-up modified staircase procedure. They reported impaired rod slope and rod sensitivity that corresponded to severity of AMD in their patient population ($n = 30$). The rod-cone break, α, was grossly abnormal. They reported cone-mediated measures, cone time constant and cone sensitivity as normal and concluded that cone function was not affected by AMD in their population.

One possible limitation of relying on RIT is that the measure confounds α with S2. Whilst it is well known that the slope of S2 is independent of the bleach intensity, it is equally well established that α is closely linked to bleach intensity, an effect clearly seen in the historical data (Hecht, 1937). The rod-cone break is also linked to test location, in that more peripherally located stimuli result in shorter α time because relatively more rods are recruited, as illustrated in Tahir et al. (2017). This, in turn, means that, in a normal population, RIT is dependent on bleach intensity and test location. As discussed in Section 1, the energy reaching the retina is dependent on pupil size and the optical density of the ocular media. Thus, where studies rely entirely on RIT, these parameters need to be controlled in some way if, for example, patients and healthy normals are to be accurately segregated. This issue was addressed by Binns et al. (2018). They concluded that a 76% bleach and a test location of $\geq 12°$ represented the best trade-off between these parameters, taking into account the duration of the test. As emphasized

in Higgins et al. (2021b), a major issue for the applicability of the RIT approach is the lack of repeatability data. This is almost certainly linked to the fact that small changes in the bleach cause an increase in α time causing excessive variability in RIT.

Jackson et al. (2014) set out to determine the sensitivity and specificity of the AdaptDx for detecting AMD. The reference standard was AMD grade based on fundus photographs. They used the AdaptDx rapid protocol, wherein RIT ≤6.5 min was classed as normal and this resulted in 91% sensitivity and 100% specificity. There were 127 patients and 21 controls. The majority of patients (n = 72) were classed as intermediate AMD whilst there were 41 with early stage AMD and 14 with advanced (AREDs step 9) disease. In that study, 14 patients failed to reach the 4 log unit cut-off criterion within the 20 min duration of the trial. As a result, the participants had to be allocated an arbitrary RIT and this was usually the total duration of the test.

A similar approach was used in Thompson et al. (2018), who compared RIT in AMD with the results of a low luminance questionnaire. In cases where RIT was longer than the total test time, this may have introduced a ceiling effect. This was evident in Owsley et al. (2017), who aimed to assess the natural history of rod-based changes in intermediate AMD over a 2-year period (n = 30). They found wide variability in the baseline RIT and in the extent to which it changed over the assessment period. Overall, there was a substantial slowing effect over the sample period. In this paper, RIT was defined as the time taken to recover to 3 log units of attenuation. However, in 7 cases, patients did not reach this criterion within the 40 min test period and were therefore labelled as 'indeterminate'. This meant the DA curve was analysed using non-linear regression instead of RIT. The values of RIT at baseline ranged from 6.8 min to 54.2 min. This changed to between 8.8 and 124.4 min at the end of the follow up period, emphasising the point about wide variability raised above and in Higgins et al. (2021b). The authors comment on the wide inter-individual variability and concede that a limitation of the technique is that it is unable to quantify the severity of the defect in cases where recovery is particularly slow.

Whether or not slowed DA can be regarded as a genuine biomarker for AMD was addressed by Owsley et al. (2016). They tested 325 normal individuals, comparing baseline results with those obtained after 3 years. They used an extended version of the AdaptDx assuming RIT ≥12.3mins to be abnormal. Participants meeting this criterion were almost twice as likely to have AMD at the end of the follow up compared with those who were classified as normal. They claimed that slowed rod-mediated DA can be regarded as a functional biomarker for early AMD. Similarly, Chen et al. (2019) used a longitudinal study to investigate SDD and slowed DA in 77 AMD patients and showed RIT to decline gradually over a four year period and the presence of SDD to be strongly associated with delayed rod-mediated DA.

In their systematic review Higgins et al. (2021b) discussed 21 papers that described the use of the AdaptDx. They point to the fact that, in 12 studies, RIT was set to the cut-off time if the patient did not recover within this period, introducing inevitable bias. One of their major concerns was with repeatability, especially in those with particularly long values of RIT. The review concludes that there is an association between slowed DA and the presence of drusen and in particular SDD. However it emphasises that this finding has not yet been sufficiently well harnessed to be regarded as a genuine biomarker for AMD. Note that a method of describing the abnormal DA curve based on 'Time to Event' or survival analysis has been used to analyse RIT data. (Higgins et al., 2021a). The technique is designed to take account of capped or censored data encountered in RIT analysis.

6.3.2. Modelling the DA curve to extract parameters

Other studies have used a more comprehensive approach to investigate links between dark adaptometry and AMD. For example, Dimitrov et al. (2008) used a battery of dynamic and static tests of rod and cone function. They developed a novel PC-based system which used filters to extend the dynamic range of a standard PC monitor. This enabled them to record full DA curves, which were analysed using two exponential functions. Separate in-house techniques were also used to assess flicker thresholds and a customised colour test. The initial study (Dimitrov et al., 2008) reported on a small population of AMD patients and age-matched normals but the same group later used the battery of tests to assess 221 patients and compare them with 109 controls (Dimitrov et al., 2011). All the tests were assessed for reproducibility and diagnostic capacity according to fundus photograph-based grading. Rod recovery yielded the most accurate diagnosis with Receiver operator curves (ROC) giving a value of area under the curve (AUC) of 0.93 +/- 0.016, the next most accurate technique being cone recovery, with a value of 0.85 +/- 0.021.

Dimitrov et al. (2012) extended this work to test 293 AMD patients and 64 age-matched normals. Again, they found that rod-based recovery was particularly sensitive to the presence of the disease. However, they reported that steady-state tests declined more slowly and were therefore able to give meaningful data across the entire range of fundus changes. In a sense, the dynamic methods were too sensitive, in that they detected the disease at a very early stage but were unable to discriminate different severity levels in more advanced cases. The authors concluded that, though slightly less sensitive at early stages of the disease, their steady-state tests were more effective at monitoring progression over the wide range of severities. They concluded that static techniques provided a more appropriate end point when assessing the effectivity of new therapies.

In the later study (Dimitrov et al., 2012), the importance of being able to measure over the entire range of disease severity was emphasized. They increased the granularity of their fundus photograph grading and included cases where the disease was bilateral. As a result of this additional analysis of the fundus grading, they were able to assess the value of combining static and dynamic psychophysical measures, which included both rod and cone function.

6.3.3. Measuring cones and cone sensitivity recovery in AMD

Phipps et al. (2003) measured static and flicker perimetry in the central field of 25 AMD patients who had normal visual acuity. They compared these results with those obtained from normal observers. They showed that the flickering target was more effective than the static target at identifying the AMD-affected eyes. Some investigations have been aimed solely at assessing cone function in AMD. For example, Gaffney et al. (2011) described the topographical distribution of a dynamic cone recovery test in AMD and Gaffney et al. (2013) investigated the effect of pre-adaptation light intensity in early AMD. Dimitrov et al. (2008) tested a small number of patients and controls and reported cone recovery rate and rod cone break (α) were of high diagnostic value. Primarily this was probably because they used a foveal target and sampled rapidly in the first part of the test to obtain a reliable measure of cone recovery function. Cone-specific abnormalities were also evident, in that their 14 Hz flicker test and colour threshold tests gave high sensitivity and specificity (AUC >0.8). In a further investigation, Dimitrov et al. (2012) noted that static tests, based on cone function, matched the fundus grading more faithfully across the entire spectrum of disease severity. As discussed above, rod recovery was highly sensitive to the early stages of the disease but was not as effective at discriminating the later stages of the disease compared with, for example, 14 Hz flicker thresholds. This point echoes the problems reported above for the RIT approach in that rod-specific abnormalities are highly sensitive but information about later stages of the disease is frequently lost due to a ceiling effect.

Grant Robinson et al. (2019) used a battery of tests and in-house methods to investigate the performance of 81 AMD patients of varying severity compared with control subjects. They confirmed that cone recovery was an effective index of AMD severity and proposed that it might be a suitable biomarker for the disease. Overall we must conclude that overlooking cone function is not advisable if a comprehensive index of dysfunction in AMD is required. As highlighted in Tahir et al. (2018)

and Dimitrov et al. (2012), tests that evaluate both cone and rod function, ideally using a dynamic technique, are likely to prove the optimum method for monitoring and staging dry AMD.

6.4. The dual arc stimulus in the investigation of AMD

In an effort to further investigate the relative importance of cone and rod abnormalities in early AMD, Tahir et al. (2018) used their dual arc stimulus to test DA in 50 AMD patients and 15 controls of similar age. The stimulus was designed to probe 2 parafoveal regions with markedly different cone and rod numbers. The technique is unique in that it allows two measures of DA that are virtually simultaneous without the need for repeated testing. This is important as it is known that carry-over effects of bleaching are inevitable and these can be expected to be particularly marked in AMD.

Tahir et al. (2018) used a non-linear curve fitting technique based on the MLP model, described in section 3, to obtain the parameters of the DA curve for each observer and confirmed the importance of S2. In their analysis, they found S2 to be the best diagnostic factor using ROC analysis (presented in Fig. 17). This was in agreement with Dimitrov et al. (2011) who reported the diagnostic value of their rod recovery rate to be the highest, yielding an ROC of 0.86 ± 0.023. One objection to using rod recovery in clinical trials was that it is time consuming and challenging to the observer. As reported in section 6.6 below, where a fast method of recording and analysing DA curves is described, the DA-based test can be completed rapidly if the data are analysed in real time.

In Tahir et al. (2018), the patient group were reasonably homogeneous in that they were graded by two of the authors according to AREDs report no 18 (Ferris et al., 2005) as either AREDs grade 2 or grade 3 and all had normal or close to normal visual acuity. Despite this, there was considerable variability in the DA curves. In fact they divided readily into two groups. In the faster group, patients completed the test within the standard 40 min. In the slower group, the test had to be extended to 60 min. The latter group in general had the more severe disease. There were marked differences between the slower (n = 23) and the faster (n = 27) groups, as illustrated in Fig. 16. Overall, sensitivity was much lower in the slower group and substantially longer α times were seen. This effect was particularly notable for the inner stimulus. The authors pointed out that the *difference* between parameters derived from the two stimuli was of particular diagnostic value.

The importance of intra-individual comparisons of this kind was emphasized by Tahir et al. (2018). Recovery functions from four selected patients were presented, to illustrate the remarkable diversity of DA curves in early AMD. In one case, the functions appeared at first sight to be normal because all parameters were well-defined and the data were of high quality. However, the values for S2 and α fell outside normal limits for the healthy group, revealing the presence of the pathology. In another case, S2 was within normal limits but α was much extended compared with normal. There were examples in which S2 was different for the inner and outer stimulus and had remarkably long values of α combined with abnormal S2. It was notable that, as revealed by the modelling, the fundamental characteristics of the DA curves were maintained in all cases: cone recovery was exponential and S2 and S3 were linear. Generally the fits to the model were of high quality with $r^2 > 0.85$.

In Fig. 17, the ROC curves for the diagnostic accuracy of the inner and outer stimuli have been calculated. As with many previous studies, e.g. Dimitrov et al. (2011), the highest ROC was obtained with the measure of rod recovery, S2. The advantage of the dual arc approach is that 2 values of ROC are obtained and, whilst they might be expected to show improvement when combined in the calculation, this does not necessarily follow. For example the outer stimulus returned higher diagnostic value than the inner and together they gave a remarkable accuracy of 0.94 ± 0.22 for S2. However, in the case of α and β, there were minimal differences in terms of accuracy for the two locations. The score for all parameters combined with both inner and outer stimuli was 0.94 ± 0.03.

6.5. Link between morphological changes and function in AMD

In a further application of the arc-shaped stimulus for determining DA, using only the inner stimulus, Rodrigo-Diaz et al. (2019) investigated the link between morphological changes and scotopic and photopic visual function. The DA parameters were compared with contrast sensitivity (CS) and visual acuity (VA) measurements so that the integrity of cone and rod function could be assessed. Morphological changes were determined from (CFP) and fundus autofluorescence (FAF) images. This paper concentrated on FAF but there are others (eg (Lains et al., 2017)) who have investigated the link between DA and OCT. The majority of the patient group were graded as 5 on a five step severity scale (Bird et al., 1995), indicating that they exhibited at least one large

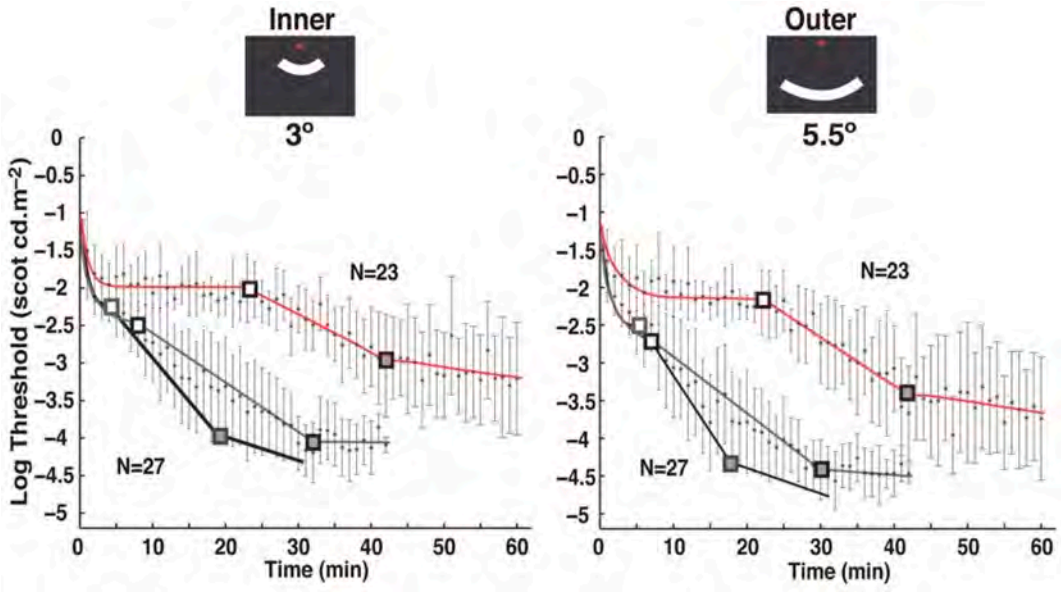

Fig. 16. Recovery functions obtained in the same session using the dual arc method. Black lines depict normal same-age observers. From Tahir et al. (2018).

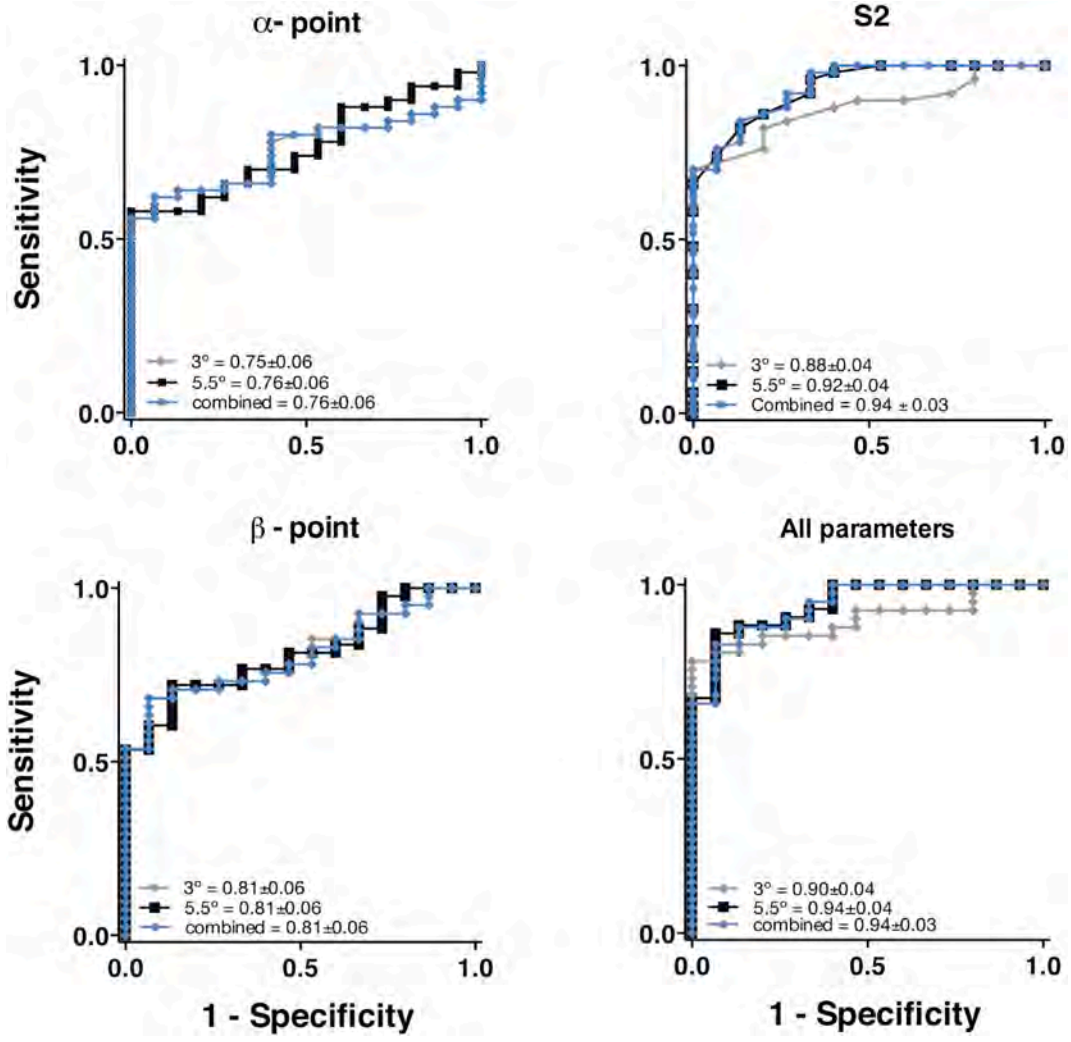

Fig. 17. ROC curves for three DA parameters, α, S2 and β and all combined, comparing data obtained from the inner and the outer stimuli (Rodrigo-Diaz, 2017).

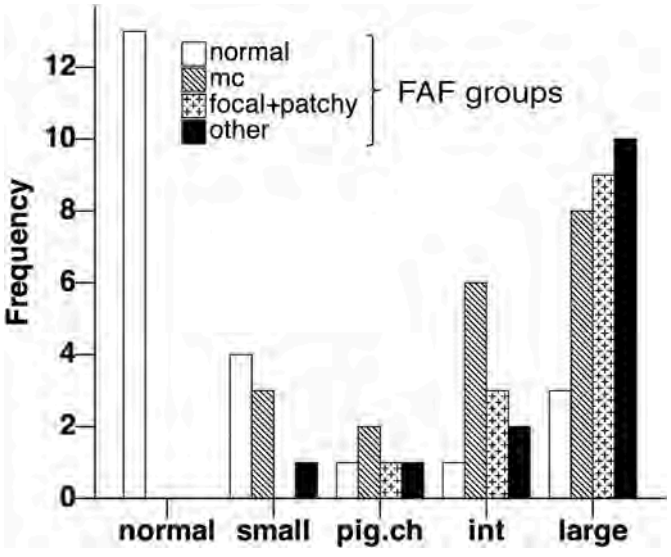

Fig. 18. Distribution of FAF groups compared with colour fundus grade (Rodrigo-Diaz et al., 2019).

(>125 μm) druse with or without pigmentary changes and non-central geographic atrophy. The FAF images were graded according to Bindewald et al. (2005). The distribution of the FAF images is presented in Fig. 18.

Consistent with previous reports, the patients with small (<63 μm) drusen displayed only minor FAF changes, but one showed a reticular pattern. Similarly, the group with pigmentary changes exhibited a wide variety of FAF changes without any particular pattern. More substantive changes in both image types corresponded as might be predicted, with most but not all intermediate AMD grade (n = 12) images showing marked FAF abnormalities. The more advanced group showed most FAF abnormalities, but note that three of these showed no colour fundus changes. Despite this group being of modest size, there was strong overall association between the two image modalities (Spearmans ρ = 0.625, P < 0.001). Note that it is almost certain that the fundus appearance and the FAF represent different expressions of the disease.

Fig. 19 illustrates the relationship between the DA parameters and the two imaging modalities. The strongest associations were between fundus photograph grade and S2 (0.61, P < 0.001). Strong correlations were also evident between S2 and FAF (0.60, P < 0.001) and between β and FAF (0.55, p < 0.001). In the case of the photopic measures, contrast sensitivity was highly correlated with FAF (−0.50, p < 0.001) and less strongly linked with CFP (−0.38, P < 0.002).

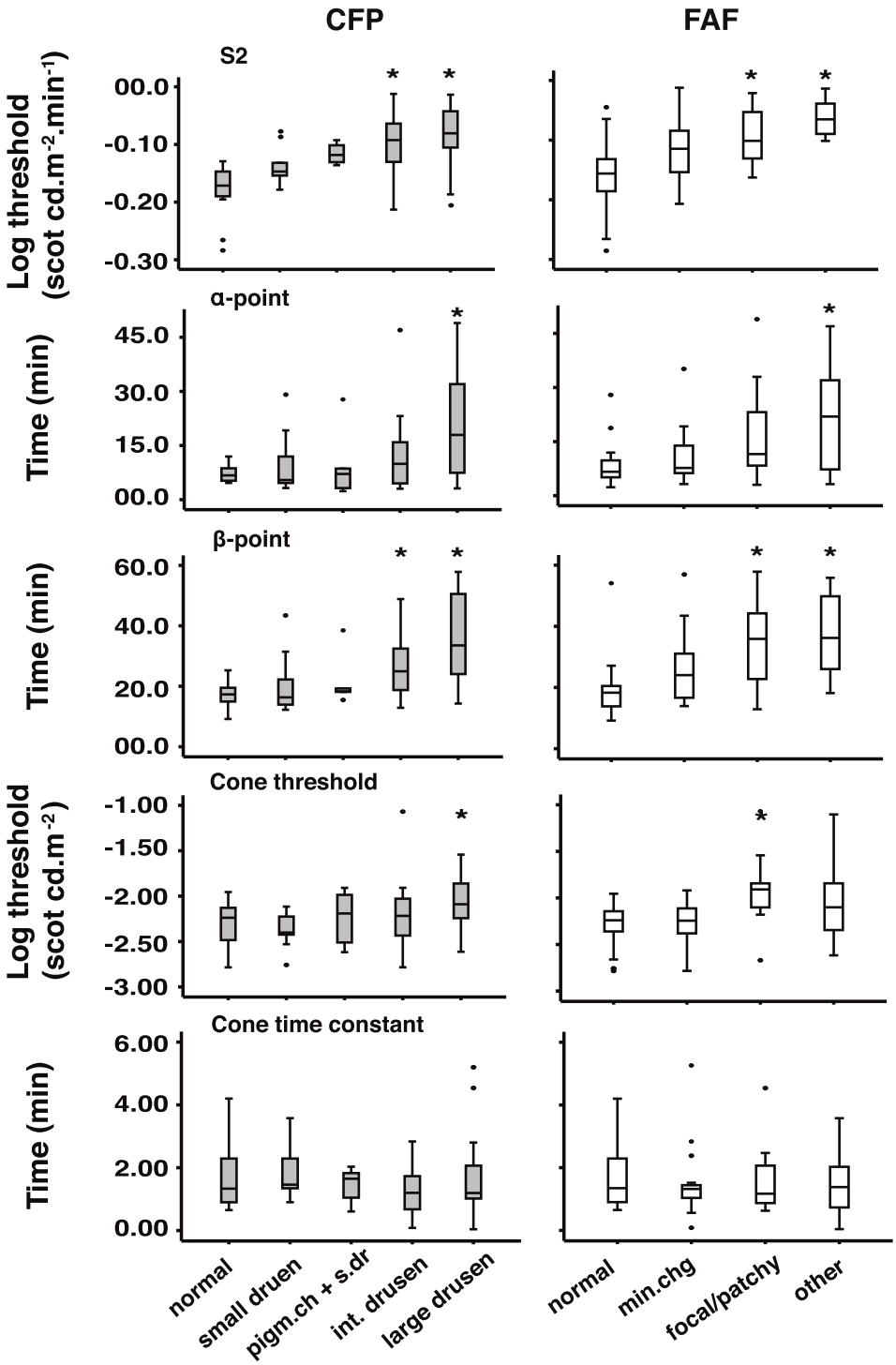

Fig. 19. The DA parameters compared with fundus photograph (CFP; left column) and FAF (right column) (Rodrigo-Diaz et al., 2019).

6.6. Retinal carotenoid supplementation

In this section a placebo-controlled intervention trial of the effects of supplementation with lutein and zeaxanthin on DA, visual acuity and contrast sensitivity is described. The retinal carotenoids lutein (L) and zeaxanthin (Z) are xanthophyll carotenoids that are entirely of dietary origin in mammals. Along with mesozeaxanthin, which is a metabolite of lutein, they make up the Macular Pigment (MP). MP accumulates in the central fovea, primarily in the photoreceptor axons. It extends radially in the Henlé, inner plexiform and nerve fibre layers of photoreceptors. This distribution has been known for many years (Snodderly et al., 1984) but was recently confirmed using Raman microscopy (Li et al., 2020). There has been much discussion in the literature regarding the possible benefits of augmenting MP with retinal carotenoid-based oral supplements (e.g. Alves-Rodrigues and Shao, 2004; Hammond et al., 2014). Some studies have described genuine improvements in visual acuity under well-controlled conditions (e.g. Ma et al., 2012; Murray et al., 2013), whilst a large scale meta-analysis did not report convincing evidence in support of any benefits (Evans and Lawrenson, 2012).

Some of the benefits described for MP are undisputed, such as the absorption of short wavelength light (Krinsky et al., 2003) and their

antioxidant properties (Khachik et al., 1997). There have been many developments in the understanding of the basic chemistry underlying the metabolism, roles and functional benefits of retinal carotenoids and there is a growing consensus that they promote retinal health. However, establishing unequivocal benefits of carotenoid supplementation across a wide population is extraordinarily complex because of the many variables involved in even the best placebo-controlled clinical trials. There are undoubted hypothetical benefits that are powerfully supported by the basic science and physiology, as discussed in a recent comprehensive review (Bernstein et al., 2016). MP can be measured using the psychophysical method of heterochromatic flicker photometry (HFP; Bone and Landrum, 2004), retinal reflectometry (Berendschot and van Norren, 2006), Raman microscopy (Bernstein et al., 1998) or an electrophysiological technique (Robson and Parry, 2008).

We present the preliminary findings of a supplementation trial with L and Z using an HFP method (van der Veen et al., 2009) to estimate MP optical density over a one-year trial period. The study was approved by the UK National Health Research Ethics Service (12/NW/0546) and registered on clinicaltrials.gov (NCT01694680). Visual acuity, contrast sensitivity (Pelli Robson chart, Haag Streit, Harlow UK) and DA, using a PC system described above, were tested on three visits. Patients were divided into placebo (P, n = 26) and Treatment (T, n = 26) groups. The placebo group (P) (mean age 72.85, SD ± 6.8) was composed of 11 participants with grade AREDS 2, and 15 AREDS 3. The Treatment group (T) (mean age 74.42, SD 7.25) composed 8 AREDS 2 and 18 AREDS 3. They were mainly recruited from advertisements in the Manchester Royal Eye Hospital and an editorial in a local newspaper.

The active daily supplementation was based on a powdered egg drink. The product contained on average 1.38 mg of lutein, 0.21 mg of zeaxanthin, and 160 mg of Docosahexaenoic Acid (DHA), an omega 3 fatty acid. This buttermilk beverage contained egg yolk obtained from chickens that had received a lutein enriched diet. (Newtricious R&D, Oirlo, The Netherlands). See Hodge et al. (2006) for a review of the possible benefits of Omega 3 in AMD. Compliance was monitored by measuring blood serum concentrations of L and Z at each visit. A food frequency questionnaire was also completed to ensure the participants did not change their diet during the trial. The DA curves were fitted with a 5-parameter model that returned cone time constant, α, S2 and β, as described in section 4.

A mixed model multivariate analysis of variance was used with Group as a fixed factor and Visit as a repeated measures factor. The model revealed statistically significant effects in the Intervention group (P = 0.02) and the Visit group (P = 0.03). There was a weak significant Intervention vs Visit interaction effect (P = 0.04). Observed power for each of these effects was greater than 0.85. These differences were further explored using Bonferroni corrected post-hoc pairwise comparisons and the results are highlighted in the figures for the different methods. Inspecting the figures for visual acuity and MPOD suggest that there is a learning effect for these parameters as revealed in the interaction effect. As might be expected this was not evident for S2, perhaps because it was a simple detection task. Supplementing with retinal carotenoids is not expected to show strong effects. Some patients appear to respond well and others less well to this type of intervention. The main benefit is that, if patients become aware of the disease early and modify their lifestyle, the progress of the disease can be slowed.

The data for the accumulation of MP and the changes in visual function over the intervention period are presented in Fig. 20. As is well known, the time course of L and Z accumulation in the retina is much slower than blood plasma with the result that the eye-related differences between P group and T group measurements are not particularly obvious at the 6 month visit.

It is important to note that, according to the post hoc analysis, the parameter known to represent rhodopsin regeneration, S2, shows a statistically significant improvement (P = 0.027) at month 12. In the case of cone function (visual acuity) there was similar pattern of improvement during the intervention period with non-significant differences between P and T groups at month 6 but stronger effects at month 12 (P = 0008). The MP improvement was similarly slow, reaching statistical significance for the final visit only (P = 0.045). The contrast sensitivity measurements were quite noisy. They show that,

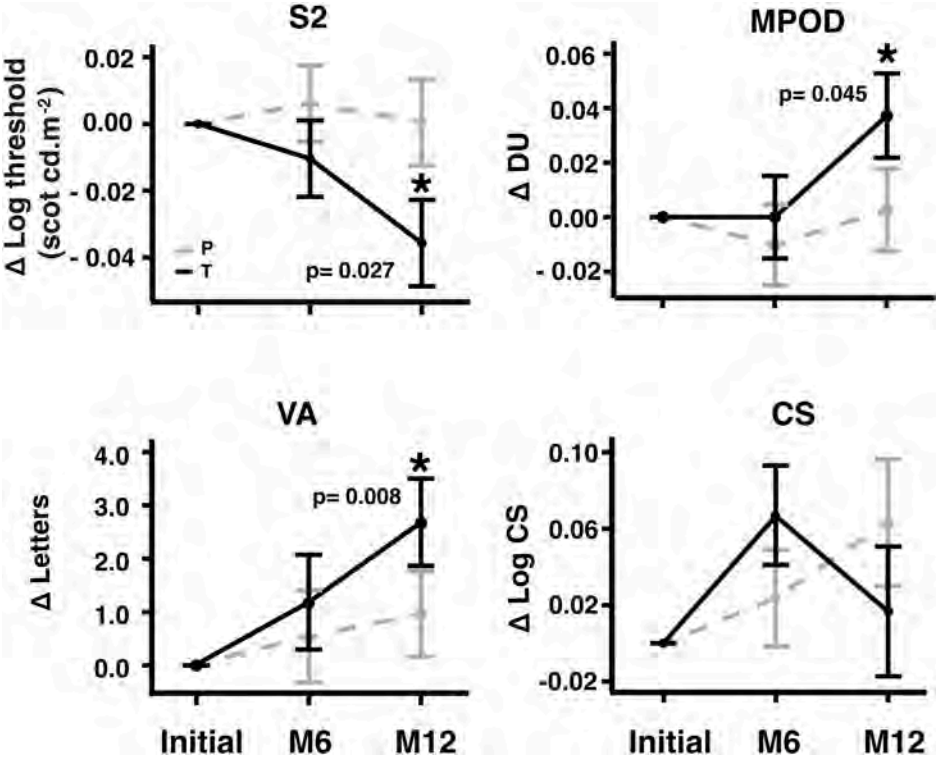

Fig. 20. Changes in rod recovery, MPOD, VA and CS over the 1 year sampling period. Results of the post hoc multiple comparisons analysis are indicated in the figures. CS remained unchanged.

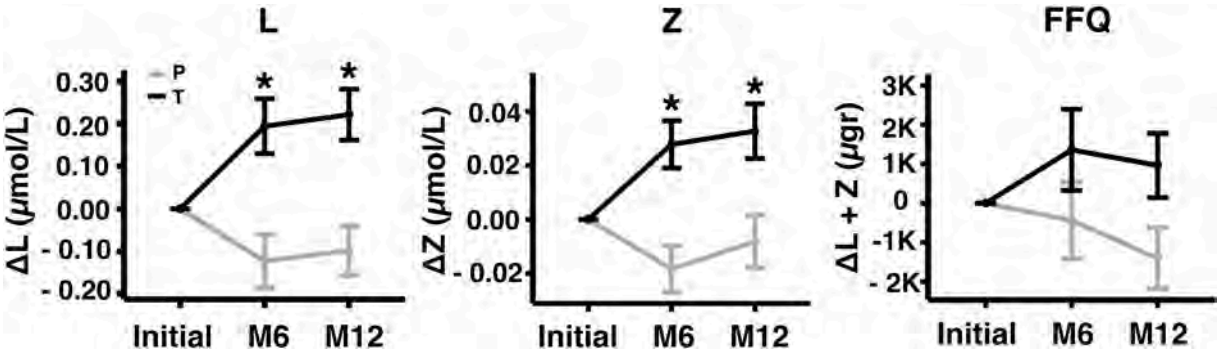

Fig. 21. Changes in blood serum levels of lutein (L) and zeaxanthin (Z) and the results of a Food Frequency (FFQ) questionnaire during the 1 year supplementation period.

based on performance on the Pelli Robson chart measurements, there were no significant changes over the course of the intervention period.

The blood serum analyses revealed quite strong effects, for both L ($P = 0.002$) and Z ($P = 0.008$), as illustrated in Fig. 21. As reported by ourselves and others, the time course for absorption in the blood stream is much more rapid than in the eye. The food frequency questionnaire data showed that diet did not change over the course of the intervention period.

Improvements in visual acuity and contrast sensitivity have been demonstrated in normal individuals in many intervention trials of retinal carotenoids. These cone-based effects are almost certainly linked to the reduction in chromatic aberration and light scatter which occur when the volume of retinal carotenoids is increased.

6.7. Clinical trial of a fast dark adaptometer

As outlined in section 4, the parameters of a DA curve can be determined using a computationally efficient extremely fast technique. Potentially, the method is a major step forward in that it means that the parameters and their associated errors can be updated in real time. Provided the computation can be performed rapidly, this can allow the parameters to be reported continuously and updated between threshold settings during the course of the test.

Here, we describe the results of a pilot case-controlled investigation of this technique. The study was registered with Clinicaltrials.gov ref NCT02090751. It was designed to test the fast on-line modelling method and incorporates a long wavelength (655 nm) dim background as described in Section 4. The fast procedure has many advantages. It is less challenging for patients than conventional methods, partly because of the red background and partly because it can be completed quickly in most cases. The real-time readout of the DA curve parameters and their errors means the testing can be terminated when the estimate of the errors reach a pre-determined satisfactory level. If an observer is healthy and responds consistently, the test may be complete within four or 5 min. If, however, the data are noisy, the technique may be extended by the operator until the software indicates the variance in the parameter estimation has reached sufficient accuracy. A further benefit is that an estimation of cone function can be obtained quickly and accurately.

As discussed in section 1, the intensity of the bleach is an important consideration when seeking to minimise the duration of the test. The technique allows bleach intensity to be customised according to age, pupil size and media optical density of the observer. Typical bleach intensity values used in the study described here were from 10^6 to 5.4×10^6 scotopic td·s which provides a relatively modest bleach of 12%–46% depending on pupil size. In this study the bleach was always >30%.

Thresholds were measured using a purpose-built light–tight surround. The target was a green (530 nm) arc-shaped target (2° wide) presented at 8° eccentricity superimposed on a deep red (655 nm) low luminance (0.05 cd•m^{-2}) background. Following the bleach the target was presented at a relatively high intensity and was gradually increased until the observer pressed a response button indicating they had detected the target. The stimulus was then reduced by 10 dB and again slowly ramped until being detected.

Forty observers were recruited from advertisements placed in local radio and newspapers and around the university. Their colour fundus photographs were classified according to the simplified AREDs scale (Ferris et al., 2005) by an ophthalmologist and one of the authors of the study. Images were enhanced by inverting and red-free filtering to ensure accurate identification of those labelled as 'unaffected'. Criteria were checked with OCT scans. This image classification of affected *vs* unaffected gave rise to two groups of twenty participants (See Fig. 22).

A 5-parameter model and purpose developed software written in R was used to characterise the DA curves using non-linear regression, as described in Section 2 and in the Appendix. All observers were able to complete the test and reported it easy to perform according to a questionnaire (not included here). S2 was obtained in all unaffected observers. The median slope of the S2 phase for the controls was −0.17 (IQR: 0.19 to −0.16) LU•min^{-1} and for the patients was −0.03 (IQR: 0.12 to 0) LU•min^{-1}

The logistic regression model to predict the difference between patients and normal observers was highly significant (intercept $P < 0.01$ and slope $P < 0.002$). For every 0.1 LU·min^{-1} improvement in S2, the Odds Ratio of belonging to the normal group was 9.3 (2.3–53). This suggested the cut-off criterion based on S2 between the groups was −1.46 dB·min^{-1}. Partitioning the data in this way meant that, of the twenty subjects with changes found by imaging, 18 had reduced S2 and two had healthy S2. Similarly, the non-affected group of twenty people had one member with a reduced rate of S2. This gave 95% sensitivity and 90% specificity as illustrated in Fig. 23.

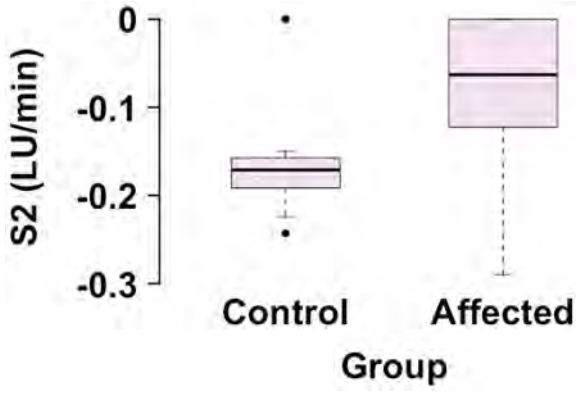

Fig. 22. Values of S2 obtained from patients and similar age normal observers. Means and 95% CIs for the two groups; controls −0.17 ± 0.04 and AMD -0.07 ± 0.08.

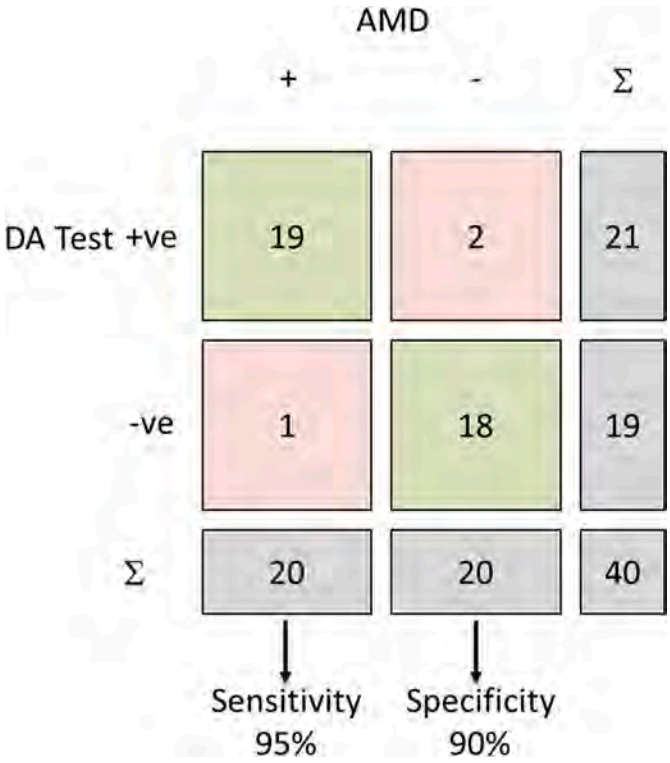

Fig. 23. Sensitivity and specificity of the rapid DA test.

Despite the small numbers in this investigation, it provides some evidence supporting many previous studies that there is a strong association between delayed DA parameters and the presence of retinal abnormalities characteristic of early AMD. The primary objective of the work was to illustrate the feasibility of applying real time modelling of DA data obtained from older normal individuals and early AMD patients of the same age. The data indicate the method is sufficiently robust to be used clinically. As others have commented, there are many unanswered questions regarding the extent to which rod-specific sensitivity recovery will be accepted as a true biomarker for early AMD. The issues are briefly discussed in the next section.

7. Summary conclusions and future directions

The recovery of sensitivity after a bleach, called dark adaptation (DA), represents multiple biochemical steps essential for the regeneration of opsins which require a new supply of 11-*cis*-retinal. The recycling of 11-*cis*-retinal is a complex process involving different enzymes and transporters in the photoreceptor outer segments and, for rods, the RPE. Bruch's membrane plays a vital role in this but also in the transport of essential nutritional material and in the disposal of waste products from the visual cycle. A separate, extremely fast, intra-retinal pathway controls the regenerative cycle of the cone opsins.

The DA curve is non-linear and composed of cone and rod-mediated stages. A quantitative analysis of the curve requires the solution of a multicomponent mathematical function. This modelling exercise returns the values of the various parameters. Previously, the process of measuring DA has been regarded as computationally cumbersome and time consuming. However, techniques have become available to improve the speed and efficiency of the analysis. This rapid analysis, described in Section 4.1, is likely to be useful in future clinical applications of the DA technique.

The fact that DA is slower in the older eye probably represents age-related compromise of the diffusional properties of Bruch's membrane. Initially, the slowing of sensitivity recovery with age seems to be confined to rods. Similar slowing of the DA curve occurs in the early stages of AMD and the ability of the technique to distinguish age-related effects from pathological changes is complicated by this phenomenon. In fact, the differences between age-related changes and pathology are far from clear-cut. Although age itself is the strongest risk factor for AMD, there is much overlap in pathological and age-related changes to all cell types in the outer retina.

It has been proposed by some that AMD is a continuum of natural aging. This is unlikely to be the case for the following reasons. First, the RPE is grossly abnormal in AMD, whereas age-related rod sensitivity and rod loss occurs in eyes where the RPE is normal and there are minimal drusen. Second, RPE abnormalities do not cause selective rod loss - cones are also impaired. It is difficult to know whether there is an intrinsic defect in rods or whether there is a subtle RPE dysfunction that affects only the ingestion and disposal of rods (Curcio et al., 1993). As discussed above, the involvement of cones might be an important factor in the staging of AMD.

The preliminary stages of AMD occur in the outer retina, where the photoreceptors have a finely balanced anatomical and physiological relationship with the retinal pigment epithelium. Bruch's membrane plays a vital role. The integrity of the outer segments of the photoreceptors relies on the exchange of many biomolecules, oxygen, nutrients and waste products through Bruch's membrane. The gradual accumulation of lipids in Bruch's membrane can be regarded as part of the normal aging process. However, with time, the structure loses its elasticity and lipoidal waste products become trapped there, compromising its biophysical properties. It therefore seems likely that targeting the lipoproteins that are retained and modified in Bruch's membrane offers the best prospect for managing AMD. One approach that has not yet been well tested is the possibility that steroidal glycosides might improve the transport pathways in Bruch's membrane. Curcio (2018) discussed skimmers and dispersants in this respect. There are some promising in vitro studies along these lines. For example (Lee et al., 2015) mounted excised Bruch's membrane preparations in a modified Ussing chamber and measured hydraulic conductivity. They reported an age-related impairment in diffusion with their technique and a twofold improvement in transport properties in response to a ginsenoside manipulation. Saponins, extracted from the ginseng plant, have been demonstrated to improve the bidirectional transport properties of Bruch's membranes in vitro and a preparation of a 200 mg oral dose is expected to remove lipoidal proteinaceous debris within six months of the start of such an intervention (Lee et al., 2020).

AMD is a major clinical problem and there is substantial impetus in clinical ophthalmology and the pharmaceutical industry to develop new therapies for arresting or at least slowing the progress of dry AMD. A primary issue is the choice of a criterion for success when these therapies undergo clinical trials. MACUSTAR deserves mention in this respect. MACUSTAR is a European Innovation Medicines Initiative involving partners from industry, hospitals and universities (Finger et al., 2019). It was established in September 2017 to develop new endpoints for clinical trials of early and intermediate AMD. Hence one goal is to develop tests capable of detecting subtle changes as dry AMD progresses. It is hoped these will give rise to new insights regarding disease progression and thereby lead to the development of effective therapies and improve the efficiency of clinical trials.

At present the only approved image-based method for assessing intervention is the expansion of geographic atrophy (GA) using autofluorescence. It may be that waiting for the onset of GA means it is too late for any intervention. There are also some possibilities, based on imaging, such as druse volume or hyperreflectivity localised to drusen (Curcio, 2018) but all approaches have limitations, partly due to the fact that changes require a long time to detect. It seems likely that morphological changes alone will not be sufficient to solve these issues and combining an image-based technique with a measure of function would be attractive. In this respect the application of Imaging Retinal Densitometry deserves mention. Using new techniques to counteract alignment difficulties, the method produces maps of rod and cone

optical density and can analyse visual pigment synthesis. It promises to reveal areas of the retina where pigment regeneration rates are compromised and therefore provide functional and morphological maps of the outer retinal integrity that would be ideal for monitoring treatment strategies (Margrain et al., 2020).

There is, therefore, a very strong case for a functional test that reflects AMD-specific morphological retinal changes. As discussed above, a dynamic measure such as DA has been shown to be most sensitive to the early stages of AMD. Certainly there are many studies in which rod-specific changes in DA appear to match the very earliest morphological changes. Assessing DA involves exposing the eye to a bleach which challenges the physiological mechanisms controlling opsin regeneration and it is this manipulation that gives the test such high sensitivity.

As reported in Tahir et al. (2018), there are abnormalities in cone function that are less conspicuous in the early stages of dry AMD but which are evident in intermediate and late dry AMD. It would therefore be important to include a measure of cone function as part of an assessment of any new therapy. Dimitrov et al. (2012) used 14 Hz flicker to achieve this. As they reported, a flickering target offers a particular challenge to the retina in that it increases metabolic demand which induces compensatory changes in retinal vasculature. They found that performance of the flicker test declined progressively across the spectrum of dry AMD disease severity.

Hence an ideal approach for assessing a new therapy would be a test mediated by central cones, e.g. a 14 Hz 2° light, combined with a subsequent measure of rod recovery based on a pre-bleach. This strategy would have the advantage of being highly sensitive to the earliest subclinical stages of the disease but remain sensitive to later stages of disease wherein the rod-based measures are less effective. This two pronged rod/cone approach would mean stabilisation or slowing of disease progression in response to new treatments could be accurately monitored regardless of the severity of disease.

It is important to note that an appropriate end-point for a clinical trial of a therapeutic strategy should also be useable in clinics for the benefit of individual patients. Despite being a much greater challenge to patients' vision and well-being than, say, glaucoma, early stage AMD patients are not well-served by the ophthalmic community. Ideally a management strategy will include appropriate imaging supported by a system capable of early detection of the condition and some form of disease staging accompanied by the application of a mathematical model for predicting disease progression in individual cases. The sole aim of this strategy would be to prevent as many individuals as possible progressing from early to severe forms of AMD.

Credit author statement

Ian J Murray: Conceptualization, Methodology, Writing – original draft, Supervision. 25%. Elena Rodrigo Diaz: Methodology. Data curation. Visualization. 20%. Jeremiah M Kelly: Software, Methodology. Data curation, Visualization. 20%. Tariq M Aslam. Conceptualization 5%. Humza J Tahir: Data curation, Visualization 5%. David Carden Conceptualization. Methodology. 10%. Laura Patryas. Data curation 5% Neil RA Parry: Conceptualization. Software. Methodology. Writing – review & editing.10%.

Acknowledgements

NRAP and TA are supported by Manchester Biomedical Research Centre and the Greater Manchester Comprehensive Local Research Network.

Some of this work was supported by Newtricious R&D B.V. (HJT and ERD) and by The National Eye Research Centre (ERD). The NIHR Invention for Innovation (i4i) Programme funded the clinical trial and JK.

IJM, DC and JK are directors of MuMac Research who developed the RapiDA technique.

We sincerely thank the reviewers for carefully reading the paper and for their many insightful comments.

APPENDIX A

Estimating parameter confidence intervals having determined. $\widehat{\theta}$

The confidence intervals for the parameters can be efficiently obtained using the Delta method (Cox, 2005). This uses a Taylor expansion of a function to determine its variance as follows

$$Y = f(\theta)$$

$$Y = f\left(\widehat{\theta}\right) + f'\left(\widehat{\theta}\right)\left(\theta - \widehat{\theta}\right) + \frac{1}{2}f''\left(\widehat{\theta}\right)\left(\theta - \widehat{\theta}\right)^2 + \tag{A1}$$

Note $Y = f(\theta)$ is equivalent to equation (5) in Section 4.

The expansion can be as large as required. The model used here assumes R in the following is small;

$$Y = f\left(\widehat{\theta}\right) + f'\left(\widehat{\theta}\right)\left(\theta - \widehat{\theta}\right) + R \tag{A2}$$

hence $Y \approx f(\widehat{\theta}) + f'(\widehat{\theta})(\theta - \widehat{\theta})$

This can be rearranged to $Y - f\left(\widehat{\theta}\right) \approx f'\left(\widehat{\theta}\right)\left(\theta - \widehat{\theta}\right)$ (A3)

If we square both sides and take the expectation (i.e. divide by degrees of freedom) we establish that the variance is

$$\left(Y - f\left(\widehat{\boldsymbol{\theta}}_i\right)\right)^2 \simeq \left(f'\left(\widehat{\boldsymbol{\theta}}_i\right)\left(\boldsymbol{\theta} - \widehat{\boldsymbol{\theta}}_i\right)\right)^2,$$

$$\sum\left(\left(Y - f\left(\widehat{\boldsymbol{\theta}}_i\right)\right)^2\right) \simeq \sum\left(\left(f'\left(\widehat{\boldsymbol{\theta}}_i\right)\left(\boldsymbol{\theta} - \widehat{\boldsymbol{\theta}}_i\right)\right)^2\right),$$

$$\sum \frac{\left(Y - f\left(\widehat{\boldsymbol{\theta}}_i\right)\right)^2}{df} \simeq f'\left(\widehat{\boldsymbol{\theta}}_i\right)^2 \sum \frac{\left(\boldsymbol{\theta} - \widehat{\boldsymbol{\theta}}_i\right)^2}{df},$$

The residuals Y_{res} are then expressed as

$$Var(Y_{res}) = \left[f'\left(\widehat{\boldsymbol{\theta}}_i\right)\right]^2 \widehat{\sigma^2}_{\widehat{\boldsymbol{\theta}}_i} \ldots \tag{A4}$$

APPENDIX B

Implementation of the technique.

The Mahroo Lamb Pugh model (Mahroo and Lamb, 2004) with the above switch function included is written as follows (cf Equation (1));

$$Y = CT + CC^{*}exp\left(\frac{x}{\tau}\right) + S2^{*}H(\alpha, x) + S3^{*}H(\beta, x), \tag{B1}$$

where $H(.,\boldsymbol{x})$ is the switch function as stated above in (3)

The vector representing the gradient $\mathbf{G} = f'(\widehat{\boldsymbol{\theta}}_i)$ is used to calculate the variance-covariance matrix along with the standard error of the residuals for a given $\widehat{\boldsymbol{\theta}}_i$

$$Var(Y_{res}) = \frac{\sum\left(\left(Y - f\left(\widehat{\boldsymbol{\theta}}_i\right)\right)^2\right.}{df},$$

$$Var(Y_{res}) = (\mathbf{G}'\mathbf{G})Var_{lin}\left(\widehat{\boldsymbol{\theta}}_i\right)$$

$$Var_{lin}\left(\widehat{\boldsymbol{\theta}}_i\right) = (\mathbf{G}'\mathbf{G})^{-1}Var(Y_{res})$$

The standard errors of the parameter estimates are given by the square root of the matrix (Var_{lin}) diagonal.

APPENDIX C

THE SWITCH FUNCTION

```
H<- function(alpha, time, K){
  1/(1 + exp(-K*(time - alpha)))
}
S <- function(alpha, time){
  out <- numeric(length(time))
  out[time>alpha] = 1
  out
}
```

This function takes values between 0 and 1.

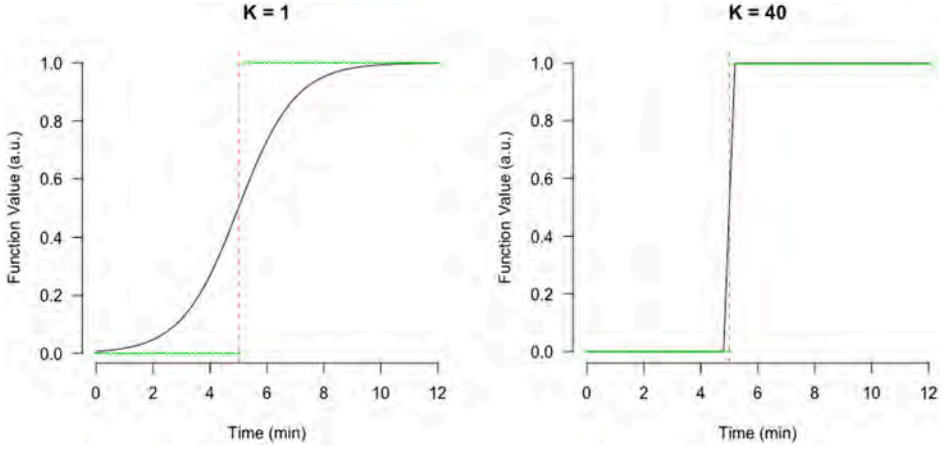

Switch function values. Both panels show the step function, in green, and the logistic switch function in black. The vertical dashed red line is the α time. The left side illustrates the effect of a lower value for 'K' while a higher value is shown on the right hand side.

References

Akaike, H., 1974. A new look at the statistical model identification. IEEE Trans. Automat. Control 19, 716–723.
Alves-Rodrigues, A., Shao, A., 2004. The science behind lutein. Toxicol. Lett. 150, 57–83.
Arnold, J.J., Heriot, W., 2007. Age related macular degeneration. Clin. Evid. 0701, 2007. https://www.ncbi.nlm.nih.gov/pmc/articles/PMC2943806/.
Arshavsky, V., 2002. Like night and day: rods and cones have different pigment regeneration pathways. Neuron 36, 1–3.
Barlow, H., 1972. Dark and light adaptation:psychophysics. In: Jameson, D., Hurvich, L. M. (Eds.), Handbook of Sensory Physiology Vol VII -4 Visual Psychophysics. Springer-Verlag, Berlin, pp. 1–28, 1972.
Bates, B.M., Watts, D.G., 1988. Nonlinear Regression Analysis and its Applications. John Wiley & Sons, New York.
Baylor, D.A., Lamb, T.D., Yau, K.W., 1979. Responses of retinal rods to single photons. J. Physiol. 288, 613–634.
Berendschot, T.T., van Norren, D., 2006. Macular pigment shows ringlike structures. Invest. Ophthalmol. Vis. Sci. 47, 709–714.
Bernstein, P.S., Li, B., Vachali, P.P., Gorusupudi, A., Shyam, R., Henriksen, B.S., Nolan, J. M., 2016. Lutein, zeaxanthin, and meso-zeaxanthin: the basic and clinical science underlying carotenoid-based nutritional interventions against ocular disease. Prog. Retin. Eye Res. 50, 34–66.
Bernstein, P.S., Yoshida, M.D., Katz, N.B., McClane, R.W., Gellermann, W., 1998. Raman detection of macular carotenoid pigments in intact human retina. Invest. Ophthalmol. Vis. Sci. 39, 2003–2011.
Besharse, J.C., Hollyfield, J.G., Rayborn, M.E., 1977. Photoreceptor outer segments: accelerated membrane renewal in rods after exposure to light. Science 196, 536–538.
Bhutto, I., Lutty, G., 2012. Understanding age-related macular degeneration (AMD): relationships between the photoreceptor/retinal pigment epithelium/Bruch's membrane/choriocapillaris complex. Mol. Aspect. Med. 33, 295–317.
Bindewald, A., Bird, A.C., Dandekar, S.S., Dolar-Szczasny, J., Dreyhaupt, J., Fitzke, F.W., Einbock, W., Holz, F.G., Jorzik, J.J., Keilhauer, C., Lois, N., Mlynski, J., Pauleikhoff, D., Staurenghi, G., Wolf, S., 2005. Classification of fundus autofluorescence patterns in early age-related macular disease. Invest. Ophthalmol. Vis. Sci. 46, 3309–3314.
Binns, A.M., Taylor, D.J., Edwards, L.A., Crabb, D.P., 2018. Determining optimal test parameters for assessing dark adaptation in people with intermediate age-related macular degeneration. Invest. Ophthalmol. Vis. Sci. 59, AMD114–AMD121.
Bird, A.C., Bressler, N.M., Bressler, S.B., Chisholm, I.H., Coscas, G., Davis, M.D., de Jong, P.T., Klaver, C.C., Klein, B.E., Klein, R., et al., 1995. An international classification and grading system for age-related maculopathy and age-related macular degeneration. The International ARM Epidemiological Study Group. Surv. Ophthalmol. 39, 367–374.
Bok, D., 1993. The retinal pigment epithelium: a versatile partner in vision. J. Cell Sci. Suppl. 17, 189–195.
Bone, R.A., Landrum, J.T., 2004. Heterochromatic flicker photometry. Arch. Biochem. Biophys. 430, 137–142.
Booij, J.C., Baas, D.C., Beisekeeva, J., Gorgels, T.G.M.F., Bergen, A.A.B., 2010. The dynamic nature of Bruch's membrane. Prog. Retin. Eye Res. 29, 1–18.
Boynton, R.M., Whitten, D.N., 1970. Visual adaptation in monkey cones: recordings of late receptor potentials. Science 170, 1423–1426.
Bressler, N.M., Bressler, S.B., Congdon, N.G., Ferris 3rd, F.L., Friedman, D.S., Klein, R., Lindblad, A.S., Milton, R.C., Seddon, J.M., Age-Related Eye Disease Study Research, G., 2003. Potential public health impact of Age-Related Eye Disease Study results: AREDS report no. 11. Arch. Ophthalmol. 121, 1621–1624.
Brown, B., Adams, A.J., Coletta, N.J., Haegerstrom-Portnoy, G., 1986. Dark adaptation in age-related maculopathy. Ophthalmic Physiol. Opt. 6, 81–84.
Bunt-Milam, A.H., Saari, J.C., 1983. Immunocytochemical localization of two retinoid-binding proteins in vertebrate retina. J. Cell Biol. 97, 703–712.
Chen, K.G., Alvarez, J.A., Yazdanie, M., Papudesu, C., Wong, W.T., Wiley, H.E., Keenan, T.D., Chew, E.Y., Ferris 3rd, F.L., Cukras, C.A., 2019. Longitudinal study of dark adaptation as a functional outcome measure for age-related macular degeneration. Ophthalmology 126, 856–865.
Chichan, H., Maus, M., Heindl, L.M., 2021. Subthreshold Nanosecond laser, from trials to real-life clinical practice: a cohort study. Clin. Ophthalmol. 15, 1887–1895.
Chirco, K.R., Sohn, E.H., Stone, E.M., Tucker, B.A., Mullins, R.F., 2017. Structural and molecular changes in the aging choroid: implications for age-related macular degeneration. Eye 31, 10–25.
Choi, E.H., Daruwalla, A., Suh, S., Leinonen, H., Palczewski, K., 2021. Retinoids in the visual cycle: role of the retinal G protein-coupled receptor. JLR (J. Lipid Res.) 62.
Chong, N.H.V., Keonin, J., Luthert, P.J., Frennesson, C.I., Weingeist, D.M., Wolf, R.L., Mullins, R.F., Hageman, G.S., 2005. Decreased thickness and integrity of the macular elastic layer of Bruch's membrane correspond to the distribution of lesions associated with age-related macular degeneration. Am. J. Pathol. 166, 241–251.
Christoforidis, J., Zhang, X., 2011. Learning effect of dark adaptation among normal subjects. Graefes Arch. Clin. Exp. Ophthalmol. 249, 1345–1352.
Clark, M.E., McGwin Jr., G., Neely, D., Feist, R., Mason 3rd, J.O., Thomley, M., White Jr., M.F., Ozaydin, B., Girkin, C.A., Owsley, C., 2011. Association between retinal thickness measured by spectral-domain optical coherence tomography (OCT) and rod-mediated dark adaptation in non-exudative age-related maculopathy. Br. J. Ophthalmol. 95, 1427–1432.
Coile, D.C., Baker, H.D., 1992. Foveal dark adaptation, photopigment regeneration, and aging. Vis. Neurosci. 8, 27–39.
Cox, C., 2005. Delta method. In: Encyclopaedia of Biostatistics. John Wiley & Sons, New York.
Curcio, C.A., 2001. Photoreceptor topography in ageing and age-related maculopathy. Eye 15, 376–383.
Curcio, C.A., 2018. Soft drusen in age-related macular degeneration: biology and targeting via the oil spill strategies. Invest. Ophthalmol. Vis. Sci. 59, AMD160–AMD181.
Curcio, C.A., Medeiros, N.E., Millican, C.L., 1996. Photoreceptor loss in age-related macular degeneration. Invest. Ophthalmol. Vis. Sci. 37, 1236–1249.
Curcio, C.A., Millican, C.L., Allen, K.A., Kalina, R.E., 1993. Aging of the human photoreceptor mosaic: evidence for selective vulnerability of rods in central retina. Invest. Ophthalmol. Vis. Sci. 34, 3278–3296.
Curcio, C.A., Owsley, C., Jackson, G.R., 2000. Spare the rods, save the cones in aging and age-related maculopathy. Invest. Ophthalmol. Vis. Sci. 41, 2015–2018.
Curcio, C.A., Sloan, K.R., Kalina, R.E., Hendrickson, A.E., 1990. Human photoreceptor topography. J. Comp. Neurol. 292, 497–523.
Das, S.R., Bhardwaj, N., Kjeldbye, H., Gouras, P., 1992. Muller cells of chicken retina synthesize 11-cis-retinol. Biochem. J. 285 (Pt 3), 907–913.
Dimitrov, P.N., Guymer, R.H., Zele, A.J., Anderson, A.J., Vingrys, A.J., 2008. Measuring rod and cone dynamics in age-related maculopathy. Invest. Ophthalmol. Vis. Sci. 49, 55–65.
Dimitrov, P.N., Robman, L.D., Varsamidis, M., Aung, K.Z., Makeyeva, G., Busija, L., Vingrys, A.J., Guymer, R.H., 2012. Relationship between clinical macular changes and retinal function in age-related macular degeneration. Invest. Ophthalmol. Vis. Sci. 53, 5213–5220.
Dimitrov, P.N., Robman, L.D., Varsamidis, M., Aung, K.Z., Makeyeva, G.A., Guymer, R. H., Vingrys, A.J., 2011. Visual function tests as potential biomarkers in age-related macular degeneration. Invest. Ophthalmol. Vis. Sci. 52, 9457–9469.
Dorey, C.K., Wu, G., Ebenstein, D., Garsd, A., Weiter, J.J., 1989. Cell loss IN the aging retina - relationship to lipofuscin accumulation and macular degeneration. Investig. Ophthalmol. Vis. Sci. 30, 1691–1699.
Evans, J.R., Lawrenson, J.G., 2012. Antioxidant vitamin and mineral supplements for preventing age-related macular degeneration. Cochrane Database Syst. Rev. CD000253.
Fain, G.L., Matthews, H.R., Cornwall, M.C., Koutalos, Y., 2001. Adaptation in vertebrate photoreceptors. Physiol. Rev. 81, 117–151.
Ferris 3rd, F.L., Wilkinson, C.P., Bird, A., Chakravarthy, U., Chew, E., Csaky, K., Sadda, S. R., Beckman Initiative for Macular Research Classification, C., 2013. Clinical classification of age-related macular degeneration. Ophthalmology 120, 844–851.
Ferris, F.L., Davis, M.D., Clemons, T.E., Lee, L.Y., Chew, E.Y., Lindblad, A.S., Milton, R.C., Bressler, S.B., Klein, R., Age-Related Eye Disease Study, R.,, 2005. A simplified severity scale for age-related macular degeneration - AREDS report no. 18. Arch. Ophthalmol. 123, 1570–1574.
Finger, R.P., Schmitz-Valckenberg, S., Schmid, M., Rubin, G.S., Dunbar, H., Tufail, A., Crabb, D.P., Binns, A., Sanchez, C.I., Margaron, P., Normand, G., Durbin, M.K., Luhmann, U.F.O., Zamiri, P., Cunha-Vaz, J., Asmus, F., Holz, F.G., on behalf of the, M.c., 2019. MACUSTAR: development and clinical validation of functional, structural, and patient-reported endpoints in intermediate age-related macular degeneration. Ophthalmologica 241, 61–72.
Gaffney, A.J., Binns, A.M., Margrain, T.H., 2011. Topography of cone dark adaptation deficits in age-related maculopathy. Optom. Vis. Sci. 88, 1080–1087.
Gaffney, A.J., Binns, A.M., Margrain, T.H., 2013. The effect of pre-adapting light intensity on dark adaptation in early age-related macular degeneration. Documenta ophthalmologica. Advances in ophthalmology 127, 191–199.
Goldstein, E.B., Wolf, B.M., 1973. Regeneration of the green-rod pigment in the isolated frog retina. Vis. Res. 13, 527–534.
Grant Robinson, D., Margrain, T., Bailey, C., Binns, A., 2019. An evaluation of a battery of functional and structural tests as predictors of likely risk of progression of Age Related Macular Degeneration. Investig. Ophthalmol. Vis. Sci. 60, 580–589.
Guymer, R., Luthert, P., Bird, A., 1999. Changes in Bruch's membrane and related structures with age. Prog. Retin. Eye Res. 18, 59–90.
Guymer, R.H., Wu, Z., Hodgson, L.A.B., Caruso, E., Brassington, K.H., Tindill, N., Aung, K.Z., McGuinness, M.B., Fletcher, E.L., Chen, F.K., Chakravarthy, U., Arnold, J.J., Heriot, W.J., Durkin, S.R., Lek, J.J., Harper, C.A., Wickremasinghe, S.S., Sandhu, S.S., Baglin, E.K., Sharangan, P., Braat, S., Luu, C.D., Laser Intervention in Early Stages of Age-Related Macular Degeneration Study, G.,, 2019. Subthreshold Nanosecond laser intervention in age-related macular degeneration: the LEAD randomized controlled clinical trial. Ophthalmology 126, 829–838.
Hammond, B.R., Fletcher, L.M., Roos, F., Wittwer, J., Schalch, W., 2014. A double-blind, placebo-controlled study on the effects of lutein and zeaxanthin on photostress recovery, glare disability, and chromatic contrast. Invest. Ophthalmol. Vis. Sci. 55, 8583–8589.
Hargrave, P.A., 2001. Rhodopsin structure, function, and topography the Friedenwald lecture. Invest. Ophthalmol. Vis. Sci. 42, 3–9.
Hecht, S., 1937. Rods, Cones, and the chemical basis of vision. Physiol. Rev. 17, 239–290.
Higgins, B.E., Montesano, G., Binns, A.M., Crabb, D.P., 2021a. Optimising assessment of dark adaptation data using time to event analysis. Sci. Rep. 11, 8323.
Higgins, B.E., Taylor, D.J., Binns, A.M., Crabb, D.P., 2021b. Are current methods of measuring dark adaptation effective in detecting the onset and progression of age-related macular degeneration? A systematic literature review. Ophthalmology and Therapy 10, 21–38.
Hodge, W.G., Schachter, H.M., Barnes, D., Pan, Y., Lowcock, E.C., Zhang, L., Sampson, M., Morrison, A., Tran, K., Miguelez, M., Lewin, G., 2006. Efficacy of omega-3 fatty acids in preventing age-related macular degeneration: a systematic review. Ophthalmology 113, 1165–1172 quiz 1172-1163, 1178.

Hurvich, L.M., Jameson, D., 1955. Some quantitative aspects of an opponent-colors theory. II. Brightness, saturation, and hue in normal and dichromatic vision. J. Opt. Soc. Am. 45, 602–616.
Hussain, A.A., Starita, C., Hodgetts, A., Marshall, J., 2010. Macromolecular diffusion characteristics of ageing human Bruch's membrane: implications for age-related macular degeneration (AMD). Exp. Eye Res. 90, 703–710.
Ingling, C.R., 1977. Spectral sensitivity of colour opponent channels. Vis. Res. 17, 1083–1089.
Jackson, G.R., Edwards, J.G., 2008. A short-duration dark adaptation protocol for assessment of age-related maculopathy. J Ocul Biol Dis Inform 1, 7–11.
Jackson, G.R., Owsley, C., Cordle, E.P., Finley, C.D., 1998. Aging and scotopic sensitivity. Vis. Res. 38, 3655–3662.
Jackson, G.R., Owsley, C., Curcio, C.A., 2002. Photoreceptor degeneration and dysfunction in aging and age-related maculopathy. Ageing Res. Rev. 1, 381–396.
Jackson, G.R., Owsley, C., McGwin Jr., G., 1999. Aging and dark adaptation. Vis. Res. 39, 3975–3982.
Jackson, G.R., Scott, I.U., Kim, I.K., Quillen, D.A., Iannaccone, A., Edwards, J.G., 2014. Diagnostic sensitivity and specificity of dark adaptometry for detection of age-related macular degeneration. Invest. Ophthalmol. Vis. Sci. 55, 1427–1431.
Jones, G.J., Crouch, R.K., Wiggert, B., Cornwall, M.C., Chader, G.J., 1989. Retinoid requirements for recovery of sensitivity after visual-pigment bleaching in isolated photoreceptors. Proc. Natl. Acad. Sci. U.S.A. 86, 9606–9610.
Kelly, J.M., 2012. Isolating Rod Function in the Human Eye. PhD Thesis University of Manchester.
Khachik, F., Bernstein, P.S., Garland, D.L., 1997. Identification of lutein and zeaxanthin oxidation products in human and monkey retinas. Invest. Ophthalmol. Vis. Sci. 38, 1802–1811.
Klein, R., Klein, B.E., Knudtson, M.D., Meuer, S.M., Swift, M., Gangnon, R.E., 2007. Fifteen-year cumulative incidence of age-related macular degeneration: the Beaver Dam Eye Study. Ophthalmology 114, 253–262.
Klein, R., Klein, B.E., Linton, K.L., 1992. Prevalence of age-related maculopathy. The beaver dam eye study. Ophthalmology 99, 933–943.
Krinsky, N.I., Landrum, J.T., Bone, R.A., 2003. Biologic mechanisms of the protective role of lutein and zeaxanthin in the eye. Annu. Rev. Nutr. 23, 171–201.
Lains, I., Miller, J.B., Park, D.H., Tsikata, E., Davoudi, S., Rahmani, S., Pierce, J., Silva, R., Chen, T.C., Kim, I.K., Vavvas, D., Miller, J.W., Husain, D., 2017. Structural changes associated with delayed dark adaptation in age-related macular degeneration. Ophthalmology 124, 1340–1352.
Lamb, T.D., 1981. The involvement of rod photoreceptors in dark adaptation. Vis. Res. 21, 1773–1782.
Lamb, T.D., 2016. Why rods and cones? Eye 30, 179–185.
Lamb, T.D., Corless, R.M., Pananos, A.D., 2015a. The kinetics of regeneration of rhodopsin under enzyme-limited availability of 11-cis retinoid. Vis. Res. 110, 23–33.
Lamb, T.D., Corless, R.M., Pananos, A.D., 2015b. The kinetics of regeneration of rhodopsin under enzyme-limited availability of 11-cis retinoid. Vis. Res. 110, 23–33.
Lamb, T.D., Pugh Jr., E.N., 2004. Dark adaptation and the retinoid cycle of vision. Prog. Retin. Eye Res. 23, 307–380.
Lamb, T.D., Pugh Jr., E.N., 2006. Phototransduction, dark adaptation, and rhodopsin regeneration the proctor lecture. Invest. Ophthalmol. Vis. Sci. 47, 5137–5152.
Lee, Y., Ahn, E.J., Hussain, A., 2020. Saponin-mediated rejuvenation of Bruch's membrane: a new strategy for intervention in dry age-related macular degeneration (AMD). In: Recent Advances and New Perspectives in Managing Macular Degeneration.
Lee, Y., Hussain, A.A., Seok, J.H., Kim, S.H., Marshall, J., 2015. Modulating the transport characteristics of bruch's membrane with steroidal glycosides and its relevance to age-related macular degeneration (AMD). Invest. Ophthalmol. Vis. Sci. 56, 8403–8418.
Li, B., George, E.W., Rognon, G.T., Gorusupudi, A., Ranganathan, A., Chang, F.Y., Shi, L., Frederick, J.M., Bernstein, P.S., 2020. Imaging lutein and zeaxanthin in the human retina with confocal resonance Raman microscopy. Proc. Natl. Acad. Sci. U.S.A. 117, 12352–12358.
Liu, J., Itagaki, Y., Ben-Shabat, S., Nakanishi, K., Sparrow, J.R., 2000. The biosynthesis of A2E, a fluorophore of aging retina, involves the formation of the precursor, A2-PE, in the photoreceptor outer segment membrane. J. Biol. Chem. 275, 29354–29360.
Ma, L., Yan, S.F., Huang, Y.M., Lu, X.R., Qian, F., Pang, H.L., Xu, X.R., Zou, Z.Y., Dong, P. C., Xiao, X., Wang, X., Sun, T.T., Dou, H.L., Lin, X.M., 2012. Effect of lutein and zeaxanthin on macular pigment and visual function in patients with early age-related macular degeneration. Ophthalmology 119, 2290–2297.
Mahroo, O.A., Lamb, T.D., 2004. Recovery of the human photopic electroretinogram after bleaching exposures: estimation of pigment regeneration kinetics. J. Physiol. 554, 417–437.
Mahroo, O.A., Lamb, T.D., 2012. Slowed recovery of human photopic ERG a-wave amplitude following intense bleaches: a slowing of cone pigment regeneration? Documenta ophthalmologica. Adv. Ophthalmol. 125, 137–147.
Margrain, T.H., Atkinson, D., Binns, A.M., Fergusson, J., Gaffney, A., Henry, D., Jones, C., Lamb, T.D., Melotte, D., Miller, C., Todd, S., Wood, A., 2020. Functional imaging of the outer retinal complex using high fidelity imaging retinal densitometry. Sci. Rep. 10, 4494.
Marshall, J., Grindle, J., Ansell, P.L., Borwein, B., 1979. Convolution in human rods: an ageing process. Br. J. Ophthalmol. 63, 181–187.
Mata, N.L., Radu, R.A., Clemmons, R.C., Travis, G.H., 2002. Isomerization and oxidation of vitamin a in cone-dominant retinas: a novel pathway for visual-pigment regeneration in daylight. Neuron 36, 69–80.
McFarland, R., Fisher, M., 1955. Alterations in dark adaptation as a function of age. J of Gerentology 10, 424–428.
McGwin Jr., G., Jackson, G.R., Owsley, C., 1999. Using nonlinear regression to estimate parameters of dark adaptation. Behav. Res. Methods Instrum. Comput. 31, 712–717.
Murray, I.J., Makridaki, M., van der Veen, R.L.P., Carden, D., Parry, N.R.A., Berendschot, T., 2013. Lutein supplementation over a one-year period in early AMD might have a mild beneficial effect on visual acuity: the CLEAR study. Investig. Ophthalmol. Vis. Sci. 54, 1781–1788.
Mustafi, D., Engel, A.H., Palczewski, K., 2009. Structure of cone photoreceptors. Prog. Retin. Eye Res. 28, 289–302.
Nelder, J.A., Mead, R., 1965. A simplex-method for function minimization. Comput. J. 7, 308–313.
Osterberg, G., 1935. Topography of the layer of rods and cones in the human retina. Acta Ophthalmol. 13, 1–103.
Owsley, C., Clark, M.E., McGwin Jr., G., 2017. Natural history of rod-mediated dark adaptation over 2 Years in intermediate age-related macular degeneration. Transl Vis Sci Technol 6, 15.
Owsley, C., Huisingh, C., Jackson, G.R., Curcio, C.A., Szalai, A.J., Dashti, N., Clark, M., Rookard, K., McCrory, M.A., Wright, T.T., Callahan, M.A., Kline, L.B., Witherspoon, C.D., McGwin Jr., G., 2014. Associations between abnormal rod-mediated dark adaptation and health and functioning in older adults with normal macular health. Invest. Ophthalmol. Vis. Sci. 55, 4776–4789.
Owsley, C., Jackson, G.R., Cideciyan, A.V., Huang, Y., Fine, S.L., Ho, A.C., Maguire, M.G., Lolley, V., Jacobson, S.G., 2000. Psychophysical evidence for rod vulnerability in age-related macular degeneration. Invest. Ophthalmol. Vis. Sci. 41, 267–273.
Owsley, C., McGwin Jr., G., Clark, M.E., Jackson, G.R., Callahan, M.A., Kline, L.B., Witherspoon, C.D., Curcio, C.A., 2016. Delayed rod-mediated dark adaptation is a functional biomarker for incident early age-related macular degeneration. Ophthalmology 123, 344–351.
Owsley, C., McGwin Jr., G., Jackson, G.R., Kallies, K., Clark, M., 2007. Cone- and rod-mediated dark adaptation impairment in age-related maculopathy. Ophthalmology 114, 1728–1735.
Palczewski, K., Kiser, P.D., 2020. Shedding new light on the generation of the visual chromophore. Proc. Natl. Acad. Sci. U.S.A. 117, 19629–19638.
Panda-Jonas, S., Jonas, J.B., Jakobczyk-Zmija, M., 1995. Retinal photoreceptor density decreases with age. Ophthalmology 102, 1853–1859.
Parry, N.R., McKeefry, D.J., Murray, I.J., 2006. Variant and invariant color perception in the near peripheral retina. JOSA A 23, 1586–1597.
Patryas, L., Parry, N.R.A., Carden, D., Baker, D.H., Kelly, J.M.F., Aslam, T., Murray, I.J., 2013. Assessment of age changes and repeatability for computer-based rod dark adaptation. Graefes Arch. Clin. Exp. Ophthalmol. 251, 1821–1827.
Pepperberg, D.R., Brown, P.K., Lurie, M., Dowling, J.E., 1978. Visual pigment and photoreceptor sensitivity in the isolated skate retina. J. Gen. Physiol. 71, 369–396.
Phipps, J.A., Guymer, R.H., Vingrys, A.J., 2003. Loss of cone function in age-related maculopathy. Invest. Ophthalmol. Vis. Sci. 44, 2277–2283.
Plantner, J.J., Le, M.L., Kean, E.L., 1991. Enzymatic deglycosylation of bovine rhodopsin. Exp. Eye Res. 53, 269–274.
Pugh, E.N., 1975. Rushton's paradox: rod dark adaptation after flash photolysis. J. Physiol. 248, 413–431.
Pumariega, N.M., Smith, R.T., Sohrab, M.A., Letien, V., Souied, E.H., 2011. A prospective study of reticular macular disease. Ophthalmology 118, 1619–1625.
Ramrattan, R.S., van der Schaft, T.L., Mooy, C.M., de Bruijn, W.C., Mulder, P.G., de Jong, P.T., 1994. Morphometric analysis of Bruch's membrane, the choriocapillaris, and the choroid in aging. Invest. Ophthalmol. Vis. Sci. 35, 2857–2864.
Reuter, T., 2011. Fifty years of dark adaptation 1961-2011. Vis. Res. 51, 2243–2262.
Robson, A.G., Parry, N.R.A., 2008. Measurement of macular pigment optical density and distribution using the steady-state visual evoked potential. Vis. Neurosci. 25 (4), 575–583.
Robson, J.G., Frishman, L.J., 1998. Dissecting the dark-adapted electroretinogram. Documenta ophthalmologica. Adv. Ophthalmol. 95, 187–215.
Rodrigo-Diaz, E., 2017. Mechanisms of Dark Adaptation and Their Link with Early Age Related Macular Degeneration. PhD. University of Manchester.
Rodrigo-Diaz, E., Tahir, H.J., Kelly, J.M., Parry, N.R.A., Aslam, T., Murray, I.J., 2019. The light and the dark of early and intermediate AMD: cone- and rod-mediated changes are linked to fundus photograph and FAF abnormalities. Investig. Ophthalmol. Vis. Sci. 60, 5070–5079.
Rudolf, M., Clark, M.E., Chimento, M.F., Li, C.M., Medeiros, N.E., Curcio, C.A., 2008. Prevalence and morphology of druse types in the macula and periphery of eyes with age-related maculopathy. Invest. Ophthalmol. Vis. Sci. 49, 1200–1209.
Rushton, W.A., Henry, G.H., 1968. Bleaching and regeneration of cone pigments in man. Vis. Res. 8, 617–631.
Rushton, W.A., Powell, D.S., 1972. The rhodopsin content and the visual threshold of human rods. Vis. Res. 12, 1073–1081.
Saari, J.C., 2012. Vitamin A metabolism in rod and cone visual cycles. In: Cousins, R.J. (Ed.), Annual Review of Nutrition, vol. 32, pp. 125–146.
Saari, J.C., Bredberg, L., Garwin, G.G., 1982. Identification of the endogenous retinoids associated with three cellular retinoid-binding proteins from bovine retina and retinal pigment epithelium. J. Biol. Chem. 257, 13329–13333.
Saari, J.C., Nawrot, M., Kennedy, B.N., Garwin, G.G., Hurley, J.B., Huang, J., Possin, D. E., Crabb, J.W., 2001. Visual cycle impairment in cellular retinaldehyde binding protein (CRALBP) knockout mice results in delayed dark adaptation. Neuron 29, 739–748.
Schadel, S.A., Heck, M., Maretzki, D., Filipek, S., Teller, D.C., Palczewski, K., Hofmann, K.P., 2003. Ligand channeling within a G-protein-coupled receptor. The entry and exit of retinals in native opsin. J. Biol. Chem. 278, 24896–24903.
Sheraidah, G., Steinmetz, R., Maguire, J., Pauleikhoff, D., Marshall, J., Bird, A.C., 1993. Correlation between lipids extracted from Bruch's membrane and age. Ophthalmology 100, 47–51.

Shevell, S.K., Martin, P.R., 2017. Color opponency: tutorial. Journal of the Optical Society of America. A, Optics, image science, and vision 34, 1099–1108.
Simon, A., Hellman, U., Wernstedt, C., Eriksson, U., 1995. The retinal pigment epithelial-specific 11-cis retinol dehydrogenase belongs to the family of short chain alcohol dehydrogenases. J. Biol. Chem. 270, 1107–1112.
Snodderly, D.M., Brown, P.K., Delori, F.C., Auran, J.D., 1984. The macular pigment. I. Absorbance spectra, localization, and discrimination from other yellow pigments in primate retinas. Invest. Ophthalmol. Vis. Sci. 25, 660–673.
Snyder, A.W., Miller, W.H., 1977. Photoreceptor diameter and spacing for highest resolving power. J. Opt. Soc. Am. 67, 696–698.
Spaide, R.F., Ooto, S., Curcio, C.A., 2018. Subretinal drusenoid deposits AKA pseudodrusen. Surv. Ophthalmol. 63, 782–815.
Steinmetz, R.L., Haimovici, R., Jubb, C., Fitzke, F.W., Bird, A.C., 1993. Symptomatic abnormalities of dark adaptation in patients with age-related Bruch's membrane change. Br. J. Ophthalmol. 77, 549–554.
Stiles, W.S., Crawford, B.H., Equivalent adaptational levels in localized retinal areas, 1932. Report of a Joint Discussion on Vision. Cambridge University Press. Physical Society of London, Cambridge, UK, 194–121.
Strauss, O., 2005. The retinal pigment epithelium in visual function. Physiol. Rev. 85, 845–881.
Sturr, J.F., Zhang, L., Taub, H.A., Hannon, D.J., Jackowski, M.M., 1997. Psychophysical evidence for losses in rod sensitivity in the aging visual system. Vis. Res. 37, 475–481.
Tahir, H.J., Rodrigo-Diaz, E., Parry, N.R., Kelly, J.M., Carden, D., Murray, I.J., 2017. Slowed dark adaptation in older eyes; effect of location. Exp. Eye Res. 155, 47–53.
Tahir, H.J., Rodrigo-Diaz, E., Parry, N.R.A., Kelly, J.M.F., Carden, D., Aslam, T.M., Murray, I.J., 2018. Slowed dark adaptation in early AMD: dual stimulus reveals scotopic and photopic abnormalities. Investig. Ophthalmol. Vis. Sci. 59, AMD202–AMD210.
Thompson, A.C., Luhmann, U.F.O., Stinnett, S.S., Vajzovic, L., Horne, A., Toth, C.A., Cousins, S.W., Lad, E.M., 2018. Association of low luminance questionnaire with objective functional measures in early and intermediate age-related macular degeneration. Investig. Ophthalmol. Vis. Sci. 59, 289–297.
Tikidji-Hamburyan, A., Reinhard, K., Storchi, R., Dietter, J., Seitter, H., Davis, K.E., Idrees, S., Mutter, M., Walmsley, L., Bedford, R.A., Ueffing, M., Ala-Laurila, P., Brown, T.M., Lucas, R.J., Munch, T.A., 2017. Rods progressively escape saturation to drive visual responses in daylight conditions. Nat. Commun. 8, 1813.
Treutwein, B., 1995. Adaptive psychophysical procedures. Vis. Res. 35, 2503–2522.
van der Veen, R.L., Berendschot, T.T., Hendrikse, F., Carden, D., Makridaki, M., Murray, I.J., 2009. A new desktop instrument for measuring macular pigment optical density based on a novel technique for setting flicker thresholds. Ophthalmic Physiol. Opt. 29, 127–137.
van Hateren, J.H., Lamb, T.D., 2006. The photocurrent response of human cones is fast and monophasic. BMC Neurosci. 7.
Wang, J.S., Kefalov, V.J., 2011. The cone-specific visual cycle. Prog. Retin. Eye Res. 30, 115–128.
Weber, E.H., 1834. De pulsu, resorptione, auditu et tactu annotationes anatomicae et physiologicae. Koehler, Leipzig, Germany.
Weiss, E., 2020. Shedding light on dark adaptation. Biochem (Lond) 42, 44–50.
Wong, W.L., Su, X., Li, X., Cheung, C.M., Klein, R., Cheng, C.Y., Wong, T.Y., 2014. Global prevalence of age-related macular degeneration and disease burden projection for 2020 and 2040: a systematic review and meta-analysis. Lancet Glob Health 2, e106–116.
Wu, Q., Blakeley, L.R., Cornwall, M.C., Crouch, R.K., Wiggert, B.N., Koutalos, Y., 2007. Interphotoreceptor retinoid-binding protein is the physiologically relevant carrier that removes retinol from rod photoreceptor outer segments. Biochemistry 46, 8669–8679.
Wyszecki, G., Stiles, W.S., 1982. Color Science: Concept and Methods, Quantitative Data and Formulae, second ed. John Wiley & Sons, Inc.